

Chapter 1

A theoretical and observational overview of brown dwarfs

Stars are large spheres of gas composed of $\sim 73\%$ of hydrogen in mass, $\sim 25\%$ of helium, and about 2% of metals, elements with atomic number larger than two like oxygen, nitrogen, carbon or iron. The core temperature and pressure are high enough to convert hydrogen into helium by the proton-proton cycle of nuclear reaction yielding sufficient energy to prevent the star from gravitational collapse. The increased number of helium atoms yields a decrease of the central pressure and temperature. The inner region is thus compressed under the gravitational pressure which dominates the nuclear pressure. This increase in density generates higher temperatures, making nuclear reactions more efficient. The consequence of this feedback cycle is that a star such as the Sun spend most of its lifetime on the main-sequence.

The most important parameter of a star is its mass because it determines its luminosity, effective temperature, radius, and lifetime. The distribution of stars with mass, known as the Initial Mass Function (hereafter IMF), is therefore of prime importance to understand star formation processes, including the conversion of interstellar matter into stars and back again. A major issue regarding the IMF concerns its universality, i.e. whether the IMF is constant in time, place, and metallicity.

When a solar-metallicity star reaches a mass below $0.072 M_{\odot}$ (Baraffe et al. 1998), the core temperature and pressure are too low to burn hydrogen stably. Objects below this mass were originally termed “black dwarfs” because the low-luminosity would hamper their detection (Kumar 1963). The name black dwarfs was also suggested for extremely old white dwarfs, but both types of objects were undetected at that time. Tarter (1976) proposed the name “brown dwarfs” because the atmospheres dominated by molecules would be difficult to understand. This denomination was quickly adopted by astronomers. However, the true colour of a brown dwarf is not brown but purple. Indeed, deuterated sodium (Na D) absorption lines are prominent in substellar objects, suppressing green wavelengths. Therefore, a mixture of red colour from a blackbody and colour from the absorption lines of Na D appear most likely, yielding a magenta colour in the optical.

After 30 years of unfruitful searches, the first unambiguous brown dwarfs were announced independently around a nearby M2 dwarf, Gl229B (Nakajima et al. 1995) and in the Pleiades, Teide 1 (Rebolo et al. 1995). Substellar objects are now routinely uncovered as companions to low-mass stars (e.g. Bouy et al. 2003), as isolated field objects (e.g. Kirkpatrick et al. 2000), as members of young open clusters (e.g. Bouvier et al. 1998), and in star-forming regions (e.g. Hillenbrand 1997). Many recent studies in young clusters have focused on the shape of the substellar IMF to investigate a possible dependence on time and environment.

This chapter reviews the current observational and theoretical knowledge on brown dwarfs and recent determinations of the substellar mass functions. This chapter is organised as follows. We define the Initial Mass Function in § 1.1 and review its determinations in the field, in young open clusters, and in star-forming regions. In § 1.2, we discuss the formation mechanisms proposed to explain the existence of brown dwarfs along with the current observational constraints. We present the physics of substellar objects in § 1.3, including the evolution of luminosity, effective temperature, and radius with time and briefly describe the composition of their atmospheres. We describe the spectral classification of ultracool dwarfs (spectral types $\geq M8$) as well as their photometric and spectroscopic characteristics in § 1.4. Finally, we give in § 1.5 an overview of the different ways to look for brown dwarfs: radial velocity, microlensing, proper motion, as companions to nearby low-mass stars, as isolated field objects, in young open clusters, and in star-forming regions.

1.1 The Initial Mass Function

1.1.1 Definitions

The stellar Initial Mass Function, $\xi(\log m)$, was defined by Salpeter (1955) as the number of stars N in a volume of space V per logarithmic mass interval $d \log m$:

$$\xi(\log m) = \frac{dN/dV}{d \log m} = \frac{dn}{d \log m} \quad \text{stars pc}^{-3} M_{\odot}$$

where $n = N/V$ represent the stellar number-density and m the mass.

Scalo (1986) defined the mass spectrum, $\xi(m)$, as the number density distribution of stars per unit mass bin. The mass spectrum, whose definition is given below, is linked to the logarithmic mass function by:

$$\xi(m) = \frac{dn}{dM} = \frac{1}{m (\ln 10)} \xi(\log m) \quad \text{stars pc}^{-3} M_{\odot}$$

The most commonly used approximations for the logarithmic and linear IMFs are power laws of index x and α , respectively:

$$\xi(\log m) = m^{-x} \quad \text{and} \quad \xi(m) = m^{-\alpha}$$

The x and α indices are related by the relation $x = \alpha - 1$.

The Initial Mass Function represents the distribution of stars with mass which were born together. However, as stars more massive than the Sun evolve off the main-sequence within the age of the Galactic disk, the present distribution of stars above $1 M_{\odot}$ differs from the primordial distribution. For stars with masses below about $0.8 M_{\odot}$, the initial mass function is well approximated by the present-day mass function.

Many studies have investigated the IMF over a large mass range in the solar neighbourhood and in young clusters. A brief overview of these estimates is given in § 1.1.3 with an emphasis on the substellar IMF. The results quoted throughout this work for the IMF derived from the observed

luminosity function will refer to the mass spectrum (unless otherwise stated) i. e. $\frac{dN}{dM} \propto M^{-\alpha}$, where α represents the slope of the power law.

1.1.2 The mass-luminosity relation

The observed quantity is the luminosity function and not the mass function. A mass-luminosity relation is required to transform the observed parameters such as fluxes and colours into physical parameters, including masses and effective temperatures. On the one hand, the mass-luminosity relation can be obtained from various evolutionary models down into the substellar regime as described below. On the other hand, a mass-luminosity relation can be derived from the observations of nearby stars with accurate trigonometric parallaxes. However, this approach is hampered by several difficulties, including the small statistics of stars with known masses and the limited depth of parallax programs. At a given age τ , the relation between the luminosity function, $\frac{dn}{dM_\lambda(m)}$, and the mass function, $\frac{dn}{dM}$, is as follows:

$$\frac{dn}{dM}(m)_\tau = \left(\frac{dn}{dM_\lambda(m)} \right) \times \left(\frac{dM_\lambda(m)}{dm} \right)_\tau$$

where $\frac{dM_\lambda(m)}{dm}$ represents the mass-luminosity relation. $M_\lambda(m)$ denotes the absolute magnitude in a given filter centred on the wavelength λ .

Two different ways exist to transform the luminosity function into a mass function. The first method involves the modelling of the luminosity function at a given wavelength to derive its mass function. The second method involves multi-colour photometry, spectroscopy, and proper motions to place each individual object in a Hertzsprung-Russell diagram in order to estimate their mass. The latter approach, which will be used in this work, requires a huge amount of telescope time. Both techniques suffer from uncertainties, including the large contamination by field stars at the low-mass end, the effect of reddening, and the uncertainties in pre-main-sequence isochrones. The most frequently used sets of isochrones to convert magnitudes into masses in young clusters are listed below:

- Palla & Stahler (1993) computed pre-main-sequence evolutionary tracks for stars in the 1.0–7.0 M_\odot mass range. The objects originated from protostars accreting from molecular clouds and were followed up to an age of 100 Myr.
- D'Antona & Mazzitelli (1994) computed pre-main-sequence evolutionary tracks for objects younger than 100 Myr over the 2.5–0.015 M_\odot mass range, assuming hydrostatic equilibrium, no mass accretion, and no mass loss.
- Burrows et al. (1997) generated non-gray solar-metallicity models predicting the colours, spectral energy distributions, and evolution of brown dwarfs and extrasolar giant planets down to 0.3 M_{Jup} from 1 Myr to 10 Gyr.
- Baraffe et al. (1998) generated non-gray solar metallicity pre-main-sequence isochrones for low-mass stars down to the substellar regime (1.4–0.020 M_\odot) spanning 1 Myr–1 Gyr in age (NextGen models). These models have been extended to 0.001 M_\odot (Dusty models; Chabrier et al. 2000b) and include the treatment of grain formation in the equation of state and in the opacity. A third set of models, the Cond models (Chabrier et al. 2000b), consider the settling of refractory species, hence eliminating their role in the opacity.

- Siess et al. (2000) presented new pre-main-sequence evolutionary tracks from 0.1 to $7.0 M_{\odot}$ at four different metallicities ($Z = 0.01–0.04$), including solar metallicity.

1.1.3 Observational determinations of the IMF

The pioneering study of the IMF by Salpeter (1955) yielded a slope with an index α equal to 2.35 between 0.4 and $10 M_{\odot}$, when expressed as the mass spectrum (Figure 1.1). Miller & Scalo (1979) and Scalo (1986) extended the IMF in the subsolar regime and approximated the mass spectrum by a three segment power law with α equal to 1.4, 2.5, and 3.3 in the mass ranges $0.1 \leq M \leq 1 M_{\odot}$, $1 \leq M \leq 10 M_{\odot}$, and $M \geq 10 M_{\odot}$, respectively (Figure 1.1). Scalo (1986) updated the determination of the mass function by Miller & Scalo (1979) using the luminosity function taking into account the latest star-count surveys in the solar neighbourhood (Wielen, Jahreiß, & Krüger 1983) and deep photometric surveys (Reid & Gilmore 1982). However, the low-mass end of the luminosity function considered by Scalo (1986) is now outdated because, on the one hand, its mass-luminosity relation is inconsistent with current stellar models, and, on the other hand, the luminosity function is not corrected for binarity.

Since the extensive study of the mass function by Scalo (1986), several breakthroughs occurred regarding the luminosity function determination. First, several deep photometric surveys were conducted along different lines of sight, yielding similar results on the shape of the luminosity function at faint magnitudes (e.g. Tinney et al., 1993). Second, progress in the modelling of the scatter observed in colour-magnitude diagrams were achieved (Kroupa, Tout, & Gilmore 1993). Third, the mass-magnitude relation was better constrained observationally to fainter magnitudes and explained theoretically (Kroupa, Tout, & Gilmore 1990). Finally, surveys dedicated to the multiplicity of field G, K, and M dwarfs (Duquennoy & Mayor 1991; Fischer & Marcy 1992) helped constraining the binary properties of nearby stars, and, thus their influence on the mass function determination.

Using the latest set of data available in the solar neighbourhood and in young clusters, Kroupa, Tout, & Gilmore (1993) extended the IMF to the hydrogen-burning limit. They represented the mass function (Figure 1.1) by a three segment power law with $\alpha = 2.7$ for stars more massive than $1 M_{\odot}$, $\alpha = 2.2$ from 0.5 to $1.0 M_{\odot}$, and $\alpha = 0.7–1.85$ in the $0.08–0.5 M_{\odot}$ mass range with a best estimate of 1.3 (Kroupa 2002). The latter estimate is in agreement with the Salpeter's estimate between 0.5 and $1 M_{\odot}$, and also above $1 M_{\odot}$.

The IMF is fairly well constrained in the $1.0–0.1 M_{\odot}$ mass range but uncertainties remain at the high and low-mass ends. For stars more massive than $15 M_{\odot}$, several complications affect the determination of the IMF, including the difficulty of spectral classification, the uncertainties on the kinematics, and the unresolved binary companions. On the low-mass end, the recent determinations of the IMF across the hydrogen-burning limit are briefly quoted below, suggesting a power law index of $\alpha = 0.5–1.0$ in the $0.5–0.03 M_{\odot}$ mass range.

Reid et al. (1999) approximated the mass function of stars within 8 parsecs by a power law with an index α ranging from 1.0 to 2.0 with a mean value of 1.3 in the $0.1–1.0 M_{\odot}$ mass range. This result was superseded by a more recent work, yielding a index of about 1.3, in agreement with the former study, as well as a change in slope in the range $0.7–1.1 M_{\odot}$ (Reid et al. 2002a). This latest estimate of the nearby mass function essentially verifies the results of Kroupa et al. (1993), yielding a consensus on the field-star mass function. Uncertainties remain nevertheless large with regard to the choice of the mass-luminosity relation for the 8-pc sample which constitute a mixture

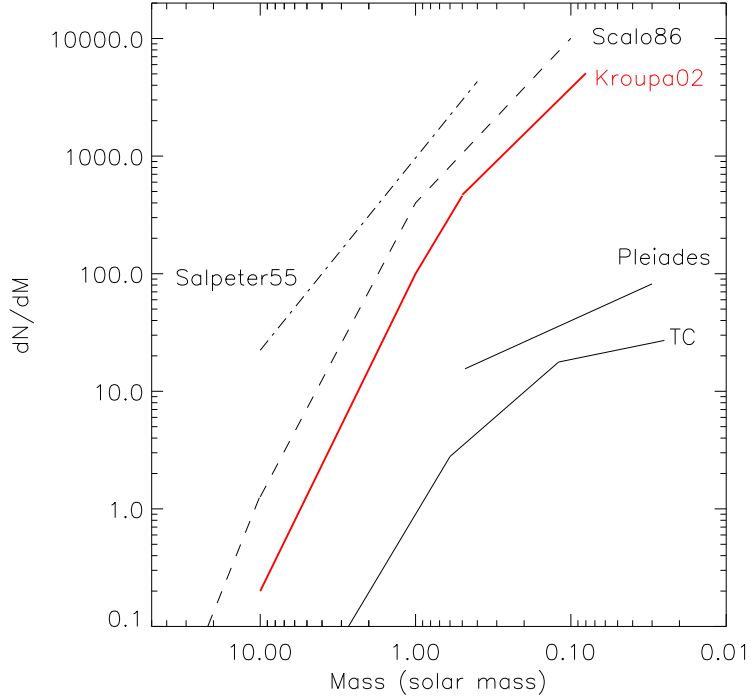


Figure 1.1: Comparison of IMF from the literature, including the pioneering estimate by Salpeter (1955; dashed-dotted line), the studies by Scalo (1986; dashed line) and Kroupa (2002; solid line). The derived mass functions for the Pleiades (Moraux et al. 2003) and the Trapezium Cluster (Muench et al. 2002) are overplotted as solid lines for comparison purposes. The different estimates are offset along the y-axis for clarity.

of stars at different ages and distances.

The advent of sensitive and wide-field optical and infrared detectors led to the discovery of a large number of substellar objects in young open clusters and in star-forming regions. In Table 1.1, we list the recent substellar IMF determinations obtained in the Pleiades (Bouvier et al. 1998; Martín et al. 1998; Tej et al. 2002; Dobbie et al. 2002; Moraux et al. 2003), α Per (Barrado y Navascués et al. 2002), σ Orionis (Béjar et al. 2001), IC348 clusters (Najita et al. 2000; Tej et al. 2002; Luhman et al. 2003b), in the Taurus cloud (Briceño et al. 2002; Luhman et al. 2003a), and in the Trapezium Cluster (McCaughrean et al. 2002a; Hillenbrand & Carpenter 2000; Luhman et al. 2000; Muench et al. 2002).

One should nevertheless keep in mind that the measured mass function will not be the same as the true IMF for several reasons. First, unresolved multiple systems will high faint companions which are not corrected for in the mass function (Kroupa 2001). The binary population evolves with time through disruption of multiple systems occurring at early ages (Kroupa 2002). In addition, the derivation of an IMF from high-mass stars down to the substellar regime is a difficult task due to dynamical evolution leading to the loss of massive and low-mass stars (Kroupa 2002). Finally, gas expulsion during the earliest times of an embedded cluster leads to violent evolution

which might affect the shape of the IMF (Kroupa et al. 2001).

To summarise, the current knowledge on the substellar IMF suggests a power law index in the range 0.5–1.0 for a large number of open clusters and star-forming regions (Table 1.1). The recent study in the low-density Taurus cloud, however, indicates a dearth of brown dwarfs compared to the Trapezium Cluster and IC348 (Briceño et al. 2002; Luhman et al. 2003a). The derived mass function peaks around $0.8 M_{\odot}$ and $0.1\text{--}0.2 M_{\odot}$ in Taurus and IC348, respectively, followed by a decline into the substellar regime when expressed in logarithmic units (Figure 1.7).

This difference might indicate a possible variation of the IMF with environment. This point is important to address the issue of the formation of brown dwarfs. Based on hydrodynamical simulations, Delgado-Donate et al. (2004) concluded that the substellar IMF is more sensitive to initial conditions than the stellar mass function, hence providing a possible explanation for the dearth of brown dwarfs observed in Taurus compared to the Trapezium Cluster. Kroupa & Bouvier (2003a) conducted N-body simulations and favoured the ejection from multiple systems to explain the variability of the substellar population between low-mass and massive star-forming regions. Those results support the conclusions from surveys dedicated to the binarity of field brown dwarfs (Burgasser et al. 2003b; Close et al. 2003; Bouy et al. 2003).

Table 1.1: The substellar IMF determinations in young open clusters and in star-forming regions. The estimates of the slope of the IMF, expressed as the mass spectrum ($\frac{dN}{dM} \propto M^{-\alpha}$), are provided for the Pleiades, α Per, σ Orionis, and IC348 clusters, the Taurus region, and Trapezium Cluster (TC). The mass range where the mass function is valid is given in solar mass (M_{\odot}). The value of α is not given for Taurus and IC348 because the authors did not attempt to fit the mass functions given in logarithmic scale. In Figure 1.7, we compare both estimates along with the determinations in the Trapezium Cluster and in σ Orionis.

Cluster	Age Myr	Distance parsecs	Mass range M_{\odot}	Mass spectrum Slope α	References
Pleiades	125 ± 8	130	0.25–0.040	1.00 ± 0.50	Martín et al. 1998
			0.40–0.040	0.60 ± 0.15	Bouvier et al. 1998
			0.50–0.055	0.50 ± 0.20	Tej et al. 2002
			0.60–0.030	0.80	Dobbie et al. 2002
			0.48–0.030	0.60 ± 0.11	Moraux et al. 2003
α Per	90 ± 10	182	0.30–0.035	0.59 ± 0.05	Barrado y Navascués et al. 2002
			0.20–0.013	0.80 ± 0.40	Béjar et al. 2001
σ Ori	3–8	352	0.30–0.030		Luhman et al. 2003b
			0.50–0.035	0.70 ± 0.20	Tej et al. 2002
			0.22–0.015	0.50	Najita et al. 2000
IC348	1–3	315	0.30–0.035		Briceño et al. 2002
			0.15–0.020	0.43	Hillenbrand & Carpenter 2000
			0.56–0.035	0.70	Luhman et al. 2000
			0.60–0.120	1.15	Muench et al. 2002
Taurus	1–2	140	0.12–0.025	0.27	Muench et al. 2002
TC	≤ 1	450			

1.2 The formation of brown dwarfs

Molecular clouds fragment into smaller entities which collapse once they exceed the thermal Jeans mass. The minimum mass reached by fragmentation is approximately $0.007 M_{\odot}$ under high density medium (Hoyle 1953; Rees 1976; Low & Lynden-Bell 1976). This lower mass limit is achieved when the collapse becomes optically-thick that is when the central object cannot radiate its heat away and is unable to fragment further. The subsequent accretion of the surrounding material on the central object leads to the formation of stars of different masses.

As a consequence, the formation mechanism of brown dwarfs appear controversial for two aspects. First, the critical mass a volume of space must contain before it will collapse under the force of its own gravity, called the Jeans mass, is typically an order of magnitude higher than the mass of a brown dwarf. Second, the central object should stop accreting in order not to reach the hydrogen-burning limit. We will briefly describe below mechanisms which have emerged over the last years to explain the existence of brown dwarfs as companions to stars, as isolated objects, and in young clusters.

1.2.1 The theory of brown dwarf formation

Turbulence

In this scenario, stars form from turbulent fragmentation of molecular clouds (for a review on this topic, refer to Mac Low & Klessen 2004). On the one hand, supersonic turbulence will prevent the collapse of large scale structures. On the other hand, the enhancement of density fluctuations on small scales will provoke their collapse. At later stages, the gravity takes over. This picture can be extended to lower masses, including substellar masses, assuming large enough density fluctuations (Klessen 2001; Padoan & Nordlund 2002).

Irradiated pre-stellar cores

A mechanism proposed by Whitworth & Zinnecker (2003; personal communication) suggests that brown dwarfs may be prestellar cores whose outer layers were eroded by the ionising radiation from OB stars. This process, obviously only possible in OB associations, requires large fluxes of ionising photons, high densities of hydrogen, and small isothermal sound speed, according to the model.

Disk instabilities

Gravitational instabilities of self gravitating protostellar disks might be responsible for the formation of brown dwarfs (Boss 1998, 2000; Li 2002). The inclusion of strong magnetic fields in the disk, responsible for an efficient cooling, can reduce the classical opacity-limit fragmentation (Low & Lynden-Bell 1976) by a factor of 10 to produce fragments with masses less than a Jupiter mass (Boss 2001).

The formation mechanism of brown dwarfs might be induced by star-disk (Boffin et al. 1998) and disc-disc encounters (Watkins et al. 1998a, 1998b; Lin et al. 1998) occurring at early stages with the presence of massive disks.

Star-disk interactions tend to truncate the disk and trigger its fragmentation to produce new stars, many of them ending up into multiple systems. For disk-disk interactions, the evolution

of the system is dominated by the fragmentation of the disk to produce twice or three times as many companions to the original stars as star-disk encounters. In coplanar disk-disk encounters, the disk material between the two interacting stars is swept into a shock layer that fragments to produce new objects, including brown dwarfs (Watkins et al. 1998a). Non-coplanar encounters trigger gravitational instabilities in the disk, which then fragment to form new companions (Watkins et al. 1998b).

In recent hydrodynamical calculation by Bate, Bonnell, & Bromm (2002), three quarters of brown dwarfs formed via fragmentation of gravitationally unstable disks, followed by a subsequent ejection from multiple systems.

Ejection mechanism

The dynamical ejection of the least massive component in multiple systems can account for brown dwarfs as well and is necessary to stop the accretion phase during the formation process (McDonald & Clarke 1993; Reipurth & Clarke 2001). This scenario suggests that brown dwarfs stopped accreting gas from the molecular cloud due to an early ejection from a multiple system (Reipurth & Clarke 2001), in agreement with the conclusions drawn from the hydrodynamical simulation by Bate et al. (2002) where all brown dwarfs are ejected, independent of their formation mechanism.

Delgado-Donate et al. (2003) and Sterzik & Durisen (2003) conducted modelling of the decay of non-hierarchical N-body systems to investigate the properties of each individual object after completion of the decay. The main results of these simulations, in terms of multiplicity, mass ratio and binary separation distributions of low-mass stars and brown dwarfs, can be summarised as follows:

1. Brown dwarfs are preferentially companions to low-mass stars. Pure binary brown dwarfs are predicted to be rare by the N-body simulations. If brown dwarfs are seen as companions, the primary is often a binary. The latter prediction await for observational tests. The simulation by Bate et al. (2002) formed at most one binary brown dwarf with a separation smaller than 10 AU, indicating that binary brown dwarfs should be less frequent than 5 %. This prevision contradicts recent observations suggesting a lower limit of about 10 % (Burgasser et al. 2003b; Close et al. 2003; Bouy et al. 2003). However, the present comparison of theoretical predictions and observations is hampered by small statistics.
2. The mass ratio distribution of brown dwarfs is predicted to be flat with rare extreme mass ratios, in agreement with current observations. Low-mass and brown dwarf binaries have separations smaller than 16 AU with a peak in the distribution around 4-8 AU (Burgasser et al. 2003b; Close et al. 2003; Bouy et al. 2003).
3. Velocity dispersions should be typically of a few km s^{-1} . Brown dwarfs would tend to exhibit slightly higher velocities than their stellar counterparts. This fact represents a potential explanation for the lack of low-mass stars and brown dwarfs in open clusters older than 200 Myr, in agreement with recent dynamical evolution simulations by de la Fuente Marcos & de la Fuente Marcos (2000).

Formation in circumstellar disks

Straddling the realms of stars and planets, brown dwarfs might also form within a circumstellar disk as the giant planets of our Solar System. The formation of planets in circumstellar disks is a longer process than the disk instabilities discussed earlier because the rocky core needs time to grow by accretion and become a planet. To test this scenario, Papaloizou & Terquem (2001) implemented simulations of dynamical interactions of $5 \leq N \leq 100$ planetary-mass objects within 100 AU of a solar mass star on a time-scale of about 100 orbits. At the end of the simulation, at most three planetary mass objects remained bound to the central star, the remainder objects being ejected. As those simulations do not impose an lower limit on the mass, the ejected objects could contribute to the population of planetary-mass objects uncovered in the Trapezium Cluster (Lucas & Roche 2000) and σ Orionis (Zapatero Osorio et al. 2000).

Radial velocity searches have noticed a lack of tight (≤ 3 AU) brown dwarf companion to solar-type stars at odds with the one hundred extrasolar planets discovered to date. Motivated by this ‘brown dwarf desert’, Armitage & Bonnell (2002) envisioned a scenario where brown dwarfs migrate either inwards or outwards, depending on the initial separation. For example, a $0.040 M_{\odot}$ brown dwarf would migrate inwards and merge into the central star in a few Myr if the initial orbital radius is smaller than 5 AU. For radii larger than 10 AU, where the disk is expanding, outwards migration occurs and pushes brown dwarfs out to radii of about 100 AU. As a consequence, the model predicts a reduction by a factor of 5 to 10 of tight brown dwarf companions to solar mass stars older than a few Myr, explaining thus the observed ‘brown dwarf desert’.

1.2.2 Observational constraints on the formation of brown dwarfs

To address the issue regarding the formation of brown dwarfs and constrain the proposed mechanisms (§ 1.2.1), several surveys have recently been carried out to search for disks around young brown dwarfs in various environments. The presence of disks around substellar objects will imply a star-like formation scenario. Truncated disks will favour the ejection model described by Reipurth & Clarke (2001) whereas the absence of disks will suggest a planet-like formation mechanism followed by dynamical ejection. Planets can nevertheless have their own disks from which their moon systems form due to the angular momentum of the accreting material.

The direct evidence for disks around young low-mass stars and brown dwarfs has been found using five different techniques described below:

1. Near-infrared (J at $1.25 \mu\text{m}$, H at $1.65 \mu\text{m}$, and K at $2.2 \mu\text{m}$) excess of selected members were reported in the Trapezium Cluster (McCaughrean & O’Dell 1996; Hillenbrand et al. 1998; Muench et al. 2002), ρ Ophiuchus (Wilking et al. 1999; Cushing et al. 2000), IC348 (Luhman 1999), and σ Orionis (Oliveira et al. 2002) based on their location in the ($J-H, H-K$) colour-colour diagram. The disk frequency around brown dwarfs appears lower in the σ Orionis cluster ($6 \pm 4\%$; Oliveira et al. 2002) than in the Trapezium Cluster ($65 \pm 15\%$; Muench et al. 2002), suggesting a disk lifetime lower than few Myr.
2. High-resolution spectroscopy for a large sample of spectroscopically confirmed low-mass stellar and brown dwarf members in a variety of star-forming regions, including Taurus, IC348, ρ Ophiuchus, and Upper Scorpius, showed that all of the targets exhibit moderate to strong asymmetric $\text{H}\alpha$ emission lines (Jayawardhana et al. 2002, 2003b; Muzerolle

et al. 2003; White & Basri 2003). Some objects also exhibit emission features such as OI (8446 Å), CaII (8662 Å), and HeI (6678 Å), characteristic of accretion in classical TTauri stars. Furthermore, the fraction of accretors tends to decrease with increasing age. In addition, the inferred accretion rates are lower than in TTauri stars by at least one order of magnitude and range from $10^{-9} M_{\odot} \text{ yr}^{-1}$ to $10^{-12} M_{\odot} \text{ yr}^{-1}$ (Muzerolle et al. 2003), suggesting the mass of the disk scales with the mass of the central object. Finally, Barrado y Navascués & Martín (2003) have reported similar timescales of accretion for low-mass stars and brown dwarfs.

3. Two extensive and complementary L'-band at $3.8 \mu\text{m}$ surveys were conducted in various star-forming regions and associations (ρ Oph, IC348, Chameleon I, Taurus, Upper Scorpius, σ Orionis, and TW Hydrae) to search for disk around pre-main-sequence objects with spectral types later than M5 (Liu, Najita, & Tokunaga 2003; Jayawardhana et al. 2003a). The L'-band offers two advantages compared to near-infrared (*JHK*) filters. First, the emission from the brown dwarf photosphere is lower at $3.8 \mu\text{m}$ than below $2.5 \mu\text{m}$ and, second, the dust sublimes at temperatures hotter than 1000 K. Those studies concluded that a large number of young low-mass stars and brown dwarfs harbour infrared $K-L'$ excesses correlated with strong H α emission, indicating a common formation mechanism for stars and brown dwarfs. The disk frequency decreases with increasing age, supporting the idea that disks do not survive longer than 10 Myr.
4. The first evidence for disks around young brown dwarfs were made in the mid-infrared with ISO (Infrared Space Observatory) measurements in ρ Ophiuchus (Bontemps et al. 2001) and in Chameleon I (Comerón et al. 2000; Persi et al. 2000). The spectral energy distributions of brown dwarfs in both regions were successfully fit by optically-thick flared disk models (Natta et al. 2002) with a possible extension to the planetary-mass regime (Testi et al. 2002), suggesting a common formation mechanism for stars and substellar mass objects. Mid-infrared ground-based measurements failed, however, to detect the silicate feature around $10 \mu\text{m}$ (Apai et al. 2002) predicted by flared disk models (Natta & Testi 2001), indicating that an optically-thick flat disk model might be sufficient to explain the observed fluxes. The mid-infrared spectral energy distribution of nearby old brown dwarfs was satisfactorily reproduced by a blackbody at the temperature of the photosphere, confirming the dissipation of disks within few hundred Myr.
5. The first dust continuum emission associated with young brown dwarfs belonging to the Taurus cloud and the IC348 cluster were reported by Klein et al. (2003). Upper limits of the quantity of dust were inferred around Pleiades and old field brown dwarfs and amounts for few Earth and Moon masses, respectively. Those detections suggest that planets might form around brown dwarfs. The presence of circumstellar dust around young brown dwarfs along with the discovery of binary brown dwarfs (Burgasser et al. 2003b; Close et al. 2003; Bouy et al. 2003) exclude the fragmentation of disks as major formation mechanism of brown dwarfs.

1.2.3 Conclusions on the formation of brown dwarfs

Several mechanisms have recently emerged to explain the existence of brown dwarfs, including turbulence, erosion of pre-stellar cores, protostellar disk instabilities with subsequent fragmenta-

tion and collapse, dynamical ejection from multiple systems, and in circumstellar disks. Current observations conducted in the infrared have concluded that a large fraction of brown dwarfs are surrounded by disks within the first Myr of their life as stars are. However, the L' -band and mid-infrared measurements below $15\ \mu\text{m}$ are only capable to probe the inner radii (\leq few AU) of disks around brown dwarfs.

The planet-type formation for brown dwarfs seems to be ruled out by the present observations. The ejection model proposed by Reipurth & Clarke (2001) predicts truncated circumstellar disks of a few AU in size, in agreement with the current infrared studies and N-body simulations (Kroupa & Bouvier 2003a). These results suggest that brown dwarfs and stars share a common formation mechanism. The recent observations of binary brown dwarfs (see Section 1.5.1; Burgasser et al. 2003b; Close et al. 2003; Bouy et al. 2003) and N-body simulations by Kroupa et al. (2003) suggest that brown dwarfs do not form with the same properties as stars because their binary properties do not represent a natural extension of those seen in stars. These results tend to favour the ejection mechanism proposed by Reipurth & Clarke (2001). Regarding the turbulence scenario of star formation, it remains plausible as both stellar and substellar can be formed without additional mechanism.

The next step is to determine disk sizes and masses from the (sub)millimetre wavelengths to shed light on the formation mechanism(s) of brown dwarfs. The expected fluxes from disks around young brown dwarfs are within the capabilities of future instrumentation, including the Atacama Large Millimeter Array (ALMA).

1.3 The physics of brown dwarfs

Current observations suggest that stars and brown dwarfs share a common formation mechanism (§ 1.2). How about the physics? Stars are large spheres of gas where the nuclear fusion compensates the gravitational energy, yielding a relationship $R \propto M^{0.6}$ between the mass (M) and the radius (R). As the electron degeneracy pressure becomes more and more important at the low-mass end of the main-sequence, the evolution of a brown dwarf is not dominated by thermonuclear processes. As a consequence, brown dwarfs cool off inexorably as they age.

This section is structured as follows. First, we describe the evolution of luminosity (§ 1.3.1), effective temperature (§ 1.3.2), and radius (§ 1.3.3) with age. Second, we discuss the influence of metallicity on the luminosity, temperature, and mass (§ 1.3.4). Then, we present the role of deuterium and lithium burning in brown dwarfs (§ 1.3.4). Finally, we give a brief overview of the composition of brown dwarf atmospheres (§ 1.3.6).

1.3.1 The evolution of luminosity

The top panel in Figure 1.2 depicts the evolution of luminosity of substellar mass objects ranging from $0.3\ M_{\text{Jup}}$ to $0.2\ M_{\odot}$ (Burrows et al. 2001)¹. Objects with masses below the deuterium burning limit at $0.013\ M_{\odot}$ are plotted in red, brown dwarfs from 0.013 to $0.075\ M_{\odot}$ in green, and stars in blue.

The separation between stars and brown dwarfs occurs only at age older than 1 Gyr. Indeed, stars stabilise at a given luminosity when the nuclear burning in the core compensates the loss

¹ $1\ M_{\odot} = 1047\ M_{\text{Jup}}$

of photons at the surface. To the contrary, brown dwarfs will never reach core temperatures and pressures high enough to ignite hydrogen. Only brown dwarfs more massive than $0.065 M_{\odot}$ will burn hydrogen briefly, but not stably.

The late-time (≥ 1 Gyr) evolution of luminosity of substellar objects can be approximated by the Equation 1.1 (Burrows et al. 2001):

$$L \sim 4 \times 10^{-5} L_{\odot} \left(\frac{10^9 \text{yr}}{t} \right)^{1.3} \left(\frac{M}{0.05 M_{\odot}} \right)^{2.64} \left(\frac{\kappa_R}{10^{-2} \text{cm}^2 \text{gm}^{-1}} \right)^{0.35} \quad (1.1)$$

where κ_R is an average atmospheric Rosseland opacity. The luminosity of a solar-metallicity star at the hydrogen burning limit is $6 \times 10^{-5} L_{\odot}$. According to Figure 1.2, the luminosity² of a $0.030 M_{\odot}$ object is approximately $10^{-2} L_{\odot}$ at 1 Myr falling down to $6 \times 10^{-6} L_{\odot}$ at 1 Gyr. This quick computation demonstrates why the detection of old brown dwarfs is limited to the Solar Neighbourhood whereas young substellar objects are uncovered in more distant open clusters and star-forming regions.

For comparison, the luminosity of main-sequence low-mass stars is approximately independent of age and is a weaker function of mass than for brown dwarfs as shown in Equation 1.2:

$$L_{star} \sim 10^{-3} L_{\odot} \left(\frac{M}{0.1 M_{\odot}} \right)^{2.2} \quad (1.2)$$

1.3.2 The evolution of temperature

The bottom panel in Figure 1.2 depicts the evolution of the effective temperatures of substellar mass objects spanning $0.3 M_{Jup}$ – $0.2 M_{\odot}$ in mass (Burrows et al. 2001).

If the mass is high enough, the thermonuclear power equals the total luminosity allowing the surface and core temperatures to stabilise, yielding a core temperature of about 3×10^6 K at the hydrogen-burning limit. However, the core of brown dwarfs will not achieve temperatures sufficient enough to balance nuclear burning and photon losses. Their core temperatures rise with age, reach a peak before falling down again. The peak of the core temperature is mass dependent and is given below:

$$T_c \sim 2 \times 10^6 \text{ K} \left(\frac{M}{0.05 M_{\odot}} \right)^{4/3}$$

The late-time evolution of the effective temperature of brown dwarfs is reproduced by the power-law given in Equation 1.3 (Burrows et al. 2001). The effective temperature is of prime importance in the classification schemes for brown dwarfs (Section 1.4).

$$T_{\text{eff}} \sim 1550 K \left(\frac{10^9 \text{yr}}{t} \right)^{0.32} \left(\frac{M}{0.05 M_{\odot}} \right)^{0.83} \left(\frac{\kappa_R}{10^{-2} \text{cm}^2 \text{gm}^{-1}} \right)^{0.088} \quad (1.3)$$

According to Figure 1.2, a $0.030 M_{\odot}$ mass brown dwarf has effective temperatures of approximately 2800 K and 900 K at 1 Myr and 1 Gyr, respectively.

²A calculator for brown dwarfs is available on Burrows's homepage: <http://zenith.as.arizona.edu/~burrows/>

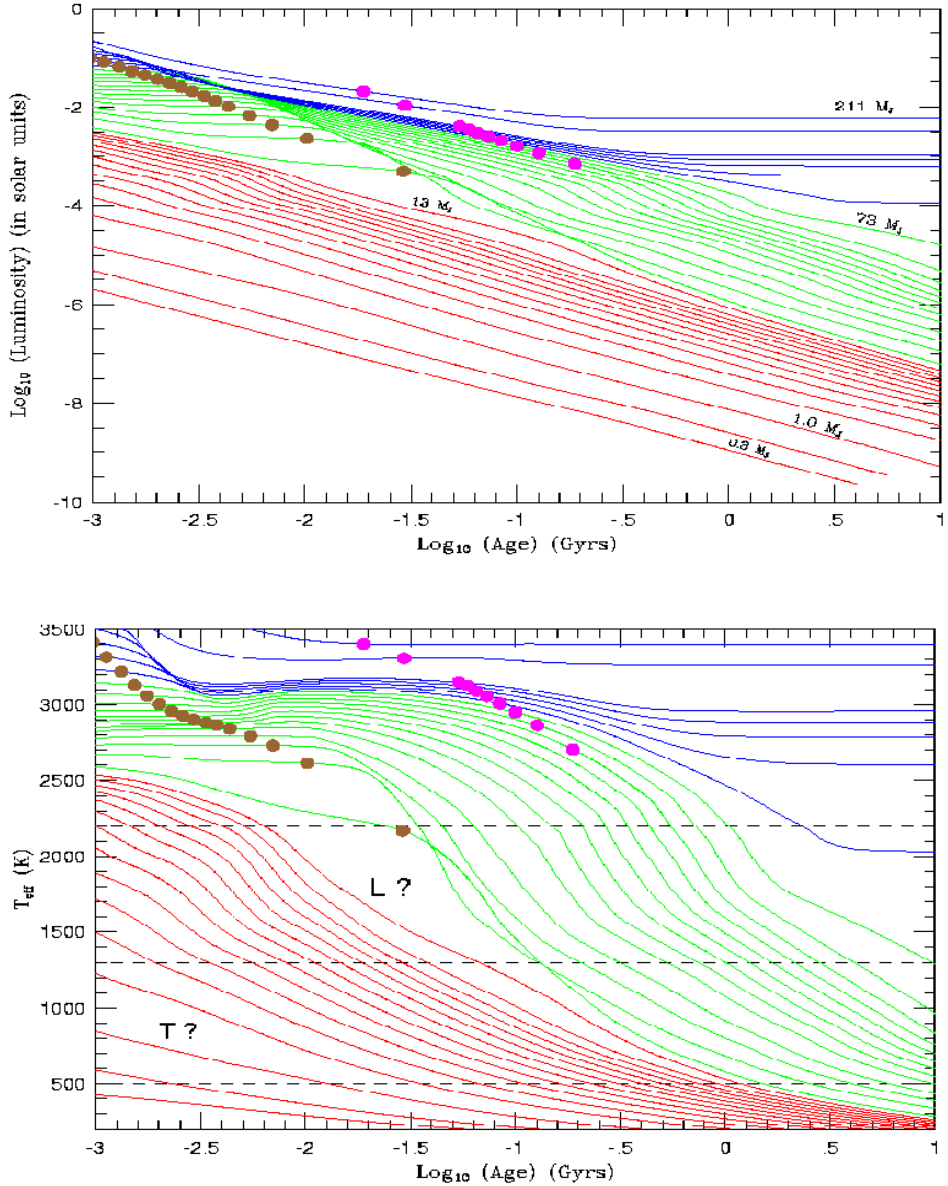


Figure 1.2: These figures, extracted from Burrows et al. (2001), depict the evolution of luminosity (top panel) and effective temperature (bottom panel) versus age of isolated solar-metallicity red dwarfs and substellar-mass objects. The stars are shown in blue, brown dwarfs above $0.013 M_{\odot}$ in green, and brown dwarfs below $0.013 M_{\odot}$ in red. The masses of objects portrayed are $0.3, 0.5, 1.0, 2.0, 3.0, 4., 5.0, 6.0, 7.0, 8.0, 9.0, 10.0, 11.0, 12.0, 13.0$, and $15.0 M_{J_{\text{up}}}$ and $0.02, 0.025, 0.03, 0.035, 0.04, 0.05, 0.06, 0.065, 0.07, 0.075, 0.08, 0.085, 0.09, 0.095, 0.1, 0.15$, and $0.2 M_{\odot}$. For a given object, the gold and magenta dots mark when 50 % of the deuterium and lithium have burned, respectively.

1.3.3 The evolution of radius

The radius decreases with age for a given mass and reaches a plateau at ages older than about 1 Gyr. For very low-mass stars, the radius increases with mass as $R \propto M^{0.6}$ but is roughly independent of age while on the main-sequence. However, the radius increases with mass for brown dwarfs younger than 100 Myr and decreases at later times. As a consequence of the competition in the equation of state between the Coulomb and the electron degeneracy, the radii of old substellar objects are independent of mass to within 30 % with the least massive ones having larger radii. Indeed, the Coulomb degeneracy yields a radius-mass relation of $R \propto M^{1/3}$ whereas the electron degeneracy (two electrons cannot occupy similar states according to the Pauli Exclusion Principle) gives $R \propto M^{-1/3}$. A more thorough analysis of the mass-radius dependence yields a relation of $R \propto M^{-1/8}$ (Chabrier & Baraffe 2000).

The radius of old substellar objects can be approximated by Equation 1.4 given below (Burrows et al. 2001).

$$R \sim 6.7 \times 10^4 \text{ km} \left(\frac{10^5}{g} \right)^{0.18} \left(\frac{T_{\text{eff}}}{1000 \text{ K}} \right)^{0.11} \quad (1.4)$$

As an example, a $0.030 M_{\odot}$ mass brown dwarf has a radius of $4.3 R_{\text{Jup}}$ and $1.0 R_{\text{Jup}}$ at 1 Myr and 1 Gyr, respectively.

1.3.4 The influence of metallicity

The properties of stars and brown dwarfs are a function of the helium fraction ($Y_{\alpha} \sim 0.25$ –0.28), the metallicity, and the opacity of the clouds in the atmosphere. Larger helium fraction, larger metallicities and larger opacities produce lower central temperature and decrease the energy from the surface, yielding more compact objects with lower masses.

The mass of a star at the hydrogen-burning limit is a function of metallicity with values between 0.070 and $0.092 M_{\odot}$ at solar and zero metallicity, respectively. Moreover, the luminosity of a star at the stellar/substellar boundary increases from 6×10^{-5} to $6 \times 10^{-3} L_{\odot}$ and its effective temperature by a factor of two from 1700 K to 3600 K with decreasing metallicity.

On the observational side, a solar-metallicity star at the hydrogen-burning limit has absolute magnitudes of $M_V = 19.5$, $M_R = 18.0$, and $M_K = 11.5$ compared to 12.8, 12.0, and 11.1 at zero-metallicity. The similarity in the K -band magnitudes is a consequence of collision-induced absorption by H_2 which suppresses the flux longwards of $2.0 \mu\text{m}$. Subdwarfs (or low-metallicity dwarfs with $[\text{Fe}/\text{H}]$ between –2.0 to –1.0) are, thus, intrinsically more luminous than normal dwarfs.

1.3.5 Deuterium and lithium burning in brown dwarfs

Substellar objects do not generate sufficient thermonuclear power to reach the hydrogen-burning limit but the most massive ones can have partial or temporary nuclear phases.

Objects more massive than $0.013 M_{\odot}$ will burn deuterium via the $p + d \rightarrow \gamma + {}^3\text{He}$ reaction. The evolution of the deuterium fraction versus age shows that all brown dwarfs more massive than $0.015 M_{\odot}$ have burned their deuterium within 30 Myr. This limit corresponds to $T_{\text{eff}} \sim 2000 \text{ K}$, spectral types around L0–L2, and luminosity of $10^{-3} L_{\odot}$.

Stars more massive than approximately $0.3 M_{\odot}$ are composed of a convective outer layer and a radiative core. Lithium is mixed in the convective part of the star but is unable to reach the central part due to the radiative region, implying that lithium is retained. On the contrary, low-mass stars ($\lesssim 0.3 M_{\odot}$) are fully convective. As a consequence, lithium can reach the central core of the star and be destroyed if the temperature is high enough.

In the substellar regime, brown dwarfs more massive than $0.065 M_{\odot}$ and older than 300 Myr will totally deplete their lithium, while substellar objects younger than 30 Myr will retain it all. Brown dwarfs more massive than $0.065 M_{\odot}$ with an age range between 30 and 300 Myr will burn lithium isotopes via the $p + ^6Li \rightarrow \alpha + ^3He$ and $p + ^7Li \rightarrow 2\alpha$ reactions. This theoretical prediction translates into an observational boundary, known as the lithium depletion boundary, between objects which exhibit lithium in absorption and those which do not. Indeed, above a given magnitude, lithium will not be spectroscopically observable because depleted, while below this magnitude limit, the lithium absorption line will appear in the spectra at 6708 \AA . This lithium depletion boundary technique, called the lithium test (Rebolo et al. 1992), was successfully applied to date open clusters, including the Pleiades (Stauffer et al. 1998), α Per (Stauffer et al. 1999), IC2391 (Barrado y Navascués et al. 2001a), and NGC 2547 (Oliveira et al. 2003).

1.3.6 Atmosphere models of low-mass stars and brown dwarfs

The main species near and above solar metallicity brown dwarf photospheres are hydrogen, helium, oxygen, carbon, and nitrogen. Strong molecular bands, absorption features, and dust are responsible for the shape and the observed spectral energy distributions of brown dwarfs. We will briefly discuss below the composition of brown dwarf atmospheres and the theoretical atmospheric models available to reproduce the emerged spectra.

- ◊ Hydrogen is predominantly in the form of H_2 and is as abundant as 90 % in brown dwarf atmospheres. Its abundance enables the presence of light hydrides (H_2O , CH_4 , NH_3 , and H_2S) as well as heavier ones, including FeH , CrH , CaH , and MgH .
- ◊ Helium is the second most abundant ($\sim 9\%$) species after hydrogen. Helium is not observed in brown dwarfs because it is chemically and spectroscopically inert.
- ◊ Oxygen is predominantly in the form of water (H_2O) and carbon monoxide (CO) but abundant enough to form of oxides, including Al_2O_3 (alumina), TiO , and VO . Titanium oxide (TiO) and vanadium oxide (VO) are responsible for the shape of M dwarf spectra but disappear at temperatures lower than $\sim 2100 \text{ K}$ and $\sim 1800 \text{ K}$, respectively, by condensing out or forming condensable species such as perovskite ($CaTiO_3$).
- ◊ Carbon is in the form of carbon monoxide (CO) at high temperatures and low pressure and of methane (CH_4) at low temperature and high pressures. Thus, CO is dominant in M dwarfs and CH_4 in T dwarfs and Jovian planets. The transition from CO to CH_4 is governed by the equation $CH_4 + H_2O \rightleftharpoons CO + 3H_2$, and occurs around 1100 K (Fegley & Lodders 1996). Carbon monoxide has been detected at $4.5\text{--}5.0 \mu\text{m}$ in Gl229B (Noll et al. 1997) whereas methane was observed at $3.3 \mu\text{m}$ in field dwarfs as early as L5, suggesting that vertical mixing play an important role in brown dwarf atmospheres (Saumon et al. 2000).
- ◊ The dominant form of nitrogen in brown dwarf atmospheres is NH_3 (ammonia) at low temperatures and N_2 at high temperatures. The transition from N_2 to NH_3 occurs at $600\text{--}700 \text{ K}$

and is governed by the equation $\text{N}_2 + 3 \text{H}_2 \rightleftharpoons \text{NH}_3$. Molecular nitrogen is invisible in the near-infrared but ammonia has already been detected in Gl229B (Noll et al. 1997), proof that vertical mixing is important (Saumon et al. 2000).

- ◊ Neutral alkalis like Na, K, Li, Cs, and Rb are less refractory than Ti, V, Ca, Si, Al, Fe, and Mg and survive in abundance in substellar atmospheres at temperatures around 1000–1500 K because of the condensation of other species. For example, lithium forms into LiCl below ~ 1400 K, making it undetectable in the optical spectra of T dwarfs.
- ◊ Metallic hydrides as FeH and CrH are present in late-M dwarfs, L dwarfs, and in M subdwarfs. CrH persists down to ~ 1500 K whereas FeH disappears below ~ 2000 – 2200 K after condensating on grains.
- ◊ Magnesium and silicium are more abundant than calcium and aluminium and form Mg/Si/O compounds, including Mg_2SiO_4 (forsterite) and MgSiO_3 (entstatite), which rain out around temperatures in the range 1800–2500 K.

Two simple cases of atmospheric models can broadly reproduce the spectral energy distributions of L and T dwarfs (see § 1.4 for a definition) over the 0.6–5.0 μm wavelength range.

- The Dusty models consider an atmosphere where the dust is uniformly mixed. These models reproduce the red optical-to-infrared and infrared colours of L dwarfs because the emerged photons are absorbed by the dust and re-emitted at longer wavelengths.
- The Cond models deal with an atmosphere where the dust has entirely settled down. These models reproduce the red optical-to-infrared and blue infrared colours of T dwarfs because the dust is located in the optically-thick region and photons are not reprocessed.

These two extreme cases of models are, however, unable to reproduce the overall spectral energy distributions of L/T transition objects (e.g. Leggett et al. 2000). The presence of clouds as those seen on Jupiter are introduced to explain the colours and spectra of L/T transition brown dwarfs.

Allard et al. (2001) proposed the “Settl” models as intermediate phase to the Dusty and Cond models, where refractory species are depleted and rain out.

Tsuji (2002) introduced the presence of a cloud in the atmosphere characterised by fixed particle sizes and constant temperatures at the bottom and the top.

Ackerman & Marley (2001) introduced the f_{rain} parameter, defined as the ratio between the sedimentation velocity and the convective velocity. A small value of f_{rain} corresponds to little sedimentation and dense clouds with vertical extent. The spectra of L/T transition objects were best reproduced by $f_{rain} = 3$ after varying this parameter from 0.1 to 10.

The L/T transition is nevertheless very sudden and still poorly understood. Cloud models, which allow to reproduce the observations, might still be in error. Possibilities of holes in the clouds, optically-thin regions with higher outward flux transmission, as well as other mechanisms should be included and tested in future atmospheric models.

To summarise, the actual atmosphere models broadly reproduce the spectral energy distributions of low-mass stars and brown dwarfs. Despite the improvement in the modelling of the atmospheres, several issues remain to be quantified, including the treatment of grain condensation,

the location of dust clouds, the molecular line lists for water and methane, the non-equilibrium chemistry, and the interplay between processes such as sedimentation and condensation. A large number of objects in the L/T transition with full wavelength coverage (0.4–5.0 μm) and high quality spectroscopy are mandatory to narrow down the uncertainties mentioned above.

1.4 Characterisation of M, L, and T dwarfs

The first release of the 2MASS database (Kirkpatrick et al. 1997), covering roughly 1 % of the whole sky, led to the discovery of several objects redder than late-M dwarfs with spectra comparable to the cool companion to the white dwarf GD165, GD165B (Becklin & Zuckerman 1988). Discoveries of cooler objects with strong methane bands and spectral features resembling those seen in the infrared spectrum of Gl229B (Oppenheimer et al. 1995) followed quickly (Burgasser et al. 1999; Strauss et al. 1999; Cuby et al. 1999).

The large number of objects cooler than the latest M dwarfs triggered the definition of two new spectral classes in addition to the Harvard Spectral classification scheme in use to classify stars (Morgan et al. 1943). Martín (1997) and Kirkpatrick et al. (1999b) proposed the letter “L” for the class of objects cooler than M dwarfs, with GD165B as a benchmark. The discovery of L dwarfs originates from the first analysis of the DENIS database (Delfosse et al. 1997) and the spectroscopic follow-up reported by Martín (1997). The classification was improved by Kirkpatrick et al. (1999b) using the discoveries from the 2MASS survey. Objects belonging to the same class as Gl229B were named “T” dwarfs and are sometimes dubbed “methane” dwarfs (Kirkpatrick et al. 1999b).

A further class of objects (the “Y” dwarfs) cooler than T dwarfs with strong ammonia absorption bands in the near or mid-infrared, characteristic of effective temperature cooler than 700 K could be expected in the near future (Burrows et al. 2001).

We will describe, in this section, the main characteristics of field M (§ 1.4.1), L (§ 1.4.2), and T (§ 1.4.3) dwarfs, including optical and near-infrared colours as well as major spectral features.

1.4.1 Spectroscopy of M dwarfs

The original MKK classification scheme defined a list of standards stars for each subclass from O stars to a spectral type of M2 (Morgan et al. 1943) with a subsequent extension to M5 (Johnson & Morgan 1953). Boeshaar (1976) extended this classification to a spectral type of M6.5 based on new later type dwarfs found in the meantime. The large number of late-M dwarfs discovered in the 1990s yielded a well-defined classification scheme for M dwarfs (Kirkpatrick et al. 1991; Kirkpatrick et al. 1999b; Martín et al. 1999b)

Optical spectra of M dwarfs (Figure 1.3) are characterised by strong oxide bands including TiO at 6320–6500 Å, 6600–6800 Å, 7050–7250 Å, 7590–7680 Å, 7670–7860 Å, 8430–8450 Å, and 8860–8940 Å and VO at 7330–7530 Å, 7850–7970 Å, and 8520–8670 Å. The atomic K I and Na I doublets at 7665/7699 Å and 8183/8195 Å, respectively, are strong as well. The H α emission line at 6563 Å, which represents a measure of chromospheric activity in M dwarfs, reaches a peak at around M6–M7 in spectral type and drops significantly towards later types (Hawley et al. 1996). The lithium absorption line at 6708 Å is detected in some late-M dwarfs like LP944-20 (Tinney 1998), placing constraints on the age and mass of these objects. The detection of

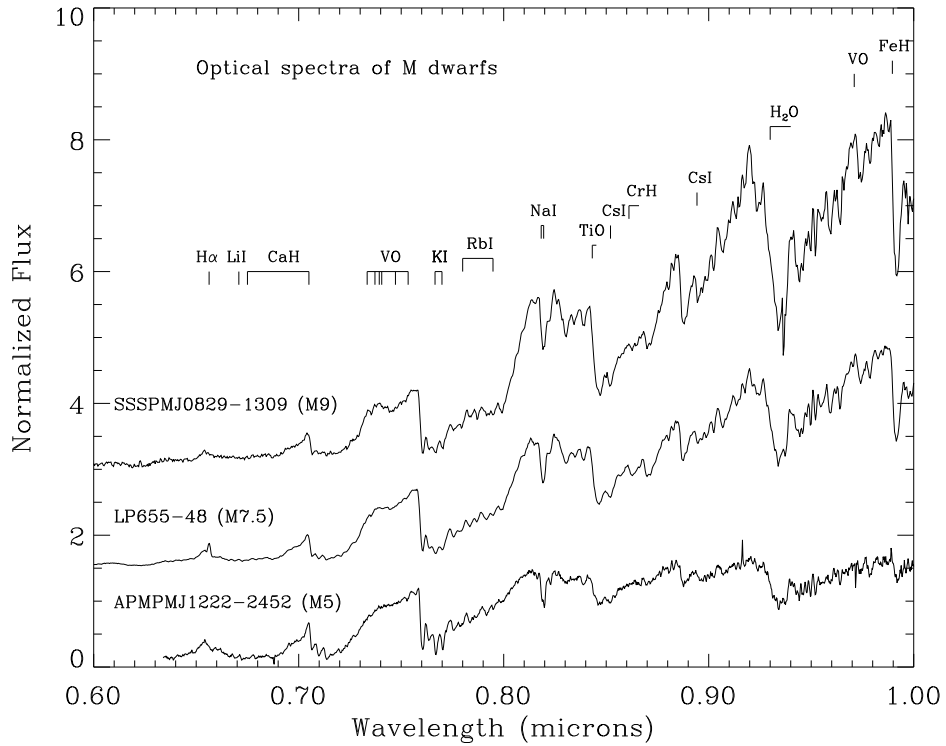


Figure 1.3: Examples of optical spectra (0.6–1.0 μm) of M dwarfs, along with the main molecular features and atomic lines. From top to bottom, the M dwarfs are SSSPM J0829-1309 (M9), LP655-48 (M7.5; McCaughean et al. 2002b), and APMPM J1222-2452 (M5) taken from our sample of proper motion objects in the Southern Sky. Optical spectra are normalised at 7500 Å and offset in intensity for clarity.

lithium in absorption at 6708 Å implies a mass less than $0.065 M_{\odot}$ and ages older than 300 Myr (Rebolo et al. 1992). The amount of lithium and the luminosity of the object provide an estimate of its mass and age (Figure 1.2).

Near-infrared spectra of M dwarfs exhibit strong H_2O , CO (2.3 μm), and FeH (1.2 μm) features as well as strong atomic lines, including KI and NaI at 1.25 and 1.51 μm , respectively.

The optical spectral classification of M dwarfs is based on spectral indices (Table 1.2) defined by Kirkpatrick et al. (1991), Kirkpatrick et al. (1999b), and Martín et al. (1999b). A complementary method useful for spectral classification is the direct comparison with template objects i.e. whose spectral type is well-determined for internal consistency.

1.4.2 Spectroscopy of L dwarfs

L dwarfs are characterised by redder optical colours ($R-I \geq 2.2$), redder optical-to-infrared colours ($I-J \geq 3.0$), and redder infrared colours ($J-K \geq 1.2$; $0.7 \leq J-H \leq 1.5$; $0.4 \leq H-K \leq 1.0$) than M dwarfs. A large scatter in colours is nevertheless observed among L dwarfs (Leggett

et al. 2000; Hawley et al. 2002). A complete list of L dwarfs with infrared magnitudes and optical spectra is available at Kirkpatrick's webpage³. Most of them are extracted from the 2MASS (e.g. Kirkpatrick et al. 2000) and SDSS (e.g. Geballe et al. 2002).

The effective temperatures of field L dwarfs range from 1300–1500 K to 2000–2200 K and their luminosities from 4×10^{-4} to $3 \times 10^{-5} L_\odot$ (Basri et al. 2000; Leggett et al. 2000). Typical uncertainties on these parameters are on the order of 15 % mostly due to uncertainties on the age of nearby ultracool dwarfs. L dwarfs represent a mixture of stars and brown dwarfs with the ones later than L5 being unambiguously substellar as theoretical models predict effective temperatures of 1700 K for a star at the hydrogen-burning limit. The detection of lithium in absorption in the optical spectrum of a L dwarf places the object in the substellar regime but not sufficient as the most massive brown dwarfs will burn hydrogen for a short period of time. As a consequence, the status of L dwarfs remain uncertain but more than one third of L dwarfs are expected to brown dwarfs (Kirkpatrick et al. 1999b). The derived density of field L dwarfs in the solar neighbourhood is estimated to $2\text{--}8 \times 10^{-3} \text{ pc}^{-3}$ (Kirkpatrick et al. 2000) compared to $2 \times 10^{-2} \text{ pc}^{-3}$ for stars in the $0.1\text{--}1.0 M_\odot$ mass range.

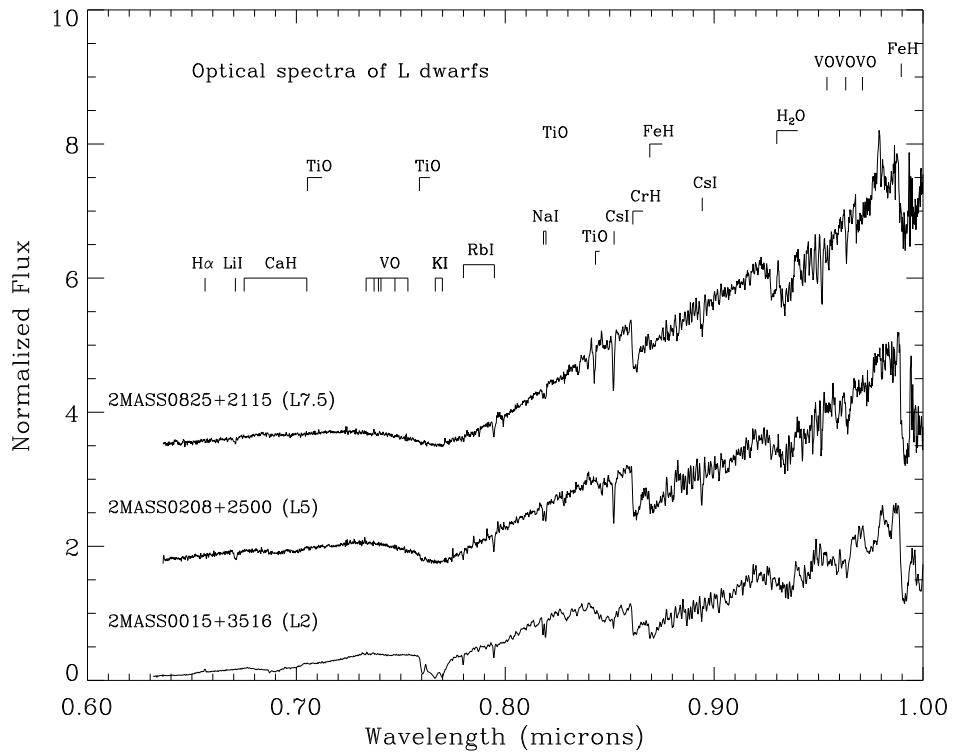


Figure 1.4: Examples of optical spectra ($0.6\text{--}1.0 \mu\text{m}$) of L dwarfs along with the main molecular features and atomic lines. From top to bottom, the L dwarfs are 2MASS0825+2115 (L7.5), 2MASS0208+2500 (L5), and 2MASS0015+3516 (L2) from Kirkpatrick et al. (2000). Optical spectra are normalised at 8250 \AA and offset in intensity for clarity.

³<http://spider.ipac.caltech.edu/staff/davy/ARCHIVE/>

The TiO and VO absorption bands, responsible for the shape of M dwarfs, disappear at lower temperatures and vanish completely by mid-L. Optical spectra of L dwarfs (Figure 1.4) are characterised by metallic hydrides such as CrH (8611 and 9969 Å), and FeH (8692 and 9896 Å), and neutral alkalis, including NaI (8183/8195 Å), KI (7665/7699 Å), RbI (7800 and 7948 Å), CsI (8521 and 8943 Å), and lithium at 6708 Å. Hydride metals, CrH and FeH, are strong around mid-L and weaken towards late types. Ground state alkali of CsI and RbI strengthen towards late types because molecules condense out in the atmosphere diminishing the veiling of atomic lines. Overall, the spectra of L dwarfs are best reproduced by the so-called “Dusty” atmosphere models of Allard et al. (2001).

The optical classification scheme of L dwarfs is based on spectral indices defined by the ratio of the summed flux in a region containing a line or a band of interest divided by the flux in a nearby continuum region. Two schemes were independently proposed by Kirkpatrick et al. (1999b) and Martín et al. (1999b).

The Kirkpatrick scheme is based on several spectral ratios which characterise the strength of oxides, metallic hydrides, and neutral alkali, as well as on comparison with template spectra of well-defined standards.

The Martín scheme relies on the so-called PC3 spectral index and on spectrum synthesis of high-resolution profiles developed by Basri et al. (2000).

There is a slight difference between both schemes particularly at low temperatures. The community tends more often to use the Kirkpatrick et al. (1999b) scheme although the PC3 index remains a good spectral type discriminant for M dwarfs and early-L dwarfs (Figure A.1 in Appendix A). Meanwhile, some authors have defined new spectral indices or adapted existent ones to their spectral resolution and/or signal-to-noise (e.g. Lépine et al. 2003b).

Table 1.2 lists the most reliable spectral indices for the spectral classification of M and L dwarfs, according to our own experience (see Chapter 2 for more details). We suggest the following “recipe” to classify M and L dwarfs in the optical with an uncertainty of half a subclass or better:

- Compute the VO-a index from Kirkpatrick et al. (1999b).
- Compute the TiO5 index from Reid et al. (1995).
- Compute the PC3 index from Martín et al. (1999b).
- Take the average of the spectral types derived from each spectral index.
- Compare the spectrum to M dwarf templates preferentially observed with the same telescope/instrument configuration as the science targets.
- Average the results obtained from both methods. If a difference larger than one subclass is found, the direct comparison with spectral templates should be favoured.

Spectral indices trace the strength of an absorption band or a spectral feature. Each wavelength of a spectrum is associated with a flux value. Those values contained in the numerator and denominator wavelength ranges are summed or averaged, according to the definition. The ratio of the two results is then computed, yielding a value for the spectral index. The output is then compared to tabulated numbers quoted in the papers where the indices are defined.

Table 1.2: Spectral indices taken from Martín et al. (1999b; hereafter M99), Reid et al. (1995; hereafter R95), and Kirkpatrick et al. (1999b; hereafter K99) for optical classification of M and L dwarfs. The different values of the flux available in the wavelength range for the numerator and denominator are summed or averaged (depending on the definition). The output of the ratio provides a value for the spectral index. This result should then be compared to values tabulated in the original papers.

Index	Numerator (Å)	Denominator (Å)	Feature	Ref
PC3	8230–8270	7540–7580	Pseudo-continuum	M99
TiO5	7126–7135	7042–7046	TiO λ 7053Å	R95
VO-a	Sum of 7350–7370 and 7550–7570	7430–7470	VO $\lambda \sim$ 7434Å	K99
CrH-a	8580–8600	8621–8641	CrH λ 8611Å	K99
Rb-b	Av of 7922.6–7932.6 and 7962.6–7972.6	7942.6–7952.6	Rb I λ 7947.6Å	K99
TiO-b	8400–8415	8435–8470	TiO λ 8432Å	K99
Cs-a	Av of 8496.1–8506.1 and 8536.1–8546.1	8516.1–8526.1	Cs I λ 8521.1Å	K99
VO-b	Sum of 7860–7880 and 8080–8100	7960–8000	VO $\lambda \sim$ 7912Å	K99

Near-infrared spectra of L dwarfs are dominated by water absorption bands at $\sim 0.95\text{ }\mu\text{m}$, $\sim 1.15\text{ }\mu\text{m}$, $1.35\text{--}1.50\text{ }\mu\text{m}$, $1.75\text{--}2.05\text{ }\mu\text{m}$, and longwards of $2.3\text{ }\mu\text{m}$, as well as by the CO band head at $2.3\text{ }\mu\text{m}$. Strong molecular bands of FeH around $1\text{ }\mu\text{m}$ and a prominent KI doublet at $1.25\text{ }\mu\text{m}$ in the *J*-band are present as well.

Several attempts have been made to provide a near-infrared classification scheme for L dwarfs in agreement with the optical scheme(s) presented above. We will briefly mention below the various indices and their applicability (Table 1.3):

- Tokunaga & Kobayashi (1999) defined two indices, K1 and K2 (Table 1.3) based on high-resolution *K*-band spectroscopy and narrow-band photometry. No clear relationship could be inferred due to the small number of objects under study. More recently, Geballe et al. (2002) concluded that these indices could be used to distinguish M, L, and T dwarfs.
- Based on very low-resolution ($R \sim 50\text{--}100$) near-infrared ($0.85\text{--}2.5\text{ }\mu\text{m}$) spectra of 26 L dwarfs with optically-determined spectral types, Testi et al. (2001) defined indices (Table 1.3) in agreement with the optical classification scheme from Kirkpatrick et al. (1999b). However, those spectral indices appear highly dependent on the instrument setup and might yield different classification at higher spectral resolution. Nevertheless, this approach remains appealing for faint brown dwarf candidates in star-forming regions invisible at optical wavelength due to the high extinction.
- Reid et al. (2001a) proposed four water-vapour indices well-correlated with the optical scheme from Kirkpatrick et al. (1999b) according to a sample of 14 L dwarfs with full $1.0\text{--}2.5\text{ }\mu\text{m}$ coverage. The best calibration with spectral type is provided by the index H_2O^B (Table 1.3) which measures the depth of absorption in the redward wing of the $1.4\text{ }\mu\text{m}$ steam band.
- Geballe et al. (2002) defined three water vapour indices and two methane indices to classify T dwarfs and extended the scheme to L dwarfs. The water vapour index at $1.5\text{ }\mu\text{m}$ is suitable for classification across the entire L-T sequence and in agreement with the optical

scheme from Kirkpatrick et al. (1999b). The CH₄ 2.2 μm and H₂O 1.5 μm spectral indices are efficient ways of classifying the L/T transition objects.

Table 1.3: Near-infrared spectral indices proposed by Tokunaga & Kobayashi (1999; TK99), Testi et al. (2001; T01), Reid et al. (2001a; R01), and Geballe et al. (2002; G02) to extend the optical classification scheme from Kirkpatrick et al. (1999b). Only the best discriminants for spectral classification are given in the case of Reid et al. (2001a) and Geballe et al. (2002).

Index	Numerator (μm)	Denominator (μm)	Ref
K1	$\langle 2.10 - 2.18 \rangle - \langle 1.96 - 2.04 \rangle$	$0.5 \times (\langle 2.10 - 2.18 \rangle + \langle 1.96 - 2.04 \rangle)$	TK99
K2	$\langle 2.20 - 2.28 \rangle - \langle 2.10 - 2.18 \rangle$	$0.5 \times (\langle 2.20 - 2.28 \rangle + \langle 2.10 - 2.18 \rangle)$	TK99
sHJ	$\langle 1.265 - 1.305 \rangle - \langle 1.60 - 1.70 \rangle$	$0.5 \times (\langle 1.265 - 1.305 \rangle + \langle 1.60 - 1.70 \rangle)$	T01
sKJ	$\langle 1.265 - 1.305 \rangle - \langle 2.12 - 2.16 \rangle$	$0.5 \times (\langle 1.265 - 1.305 \rangle + \langle 2.12 - 2.16 \rangle)$	T01
sH ₂ O ^J	$\langle 1.265 - 1.305 \rangle - \langle 1.09 - 1.13 \rangle$	$0.5 \times (\langle 1.265 - 1.305 \rangle + \langle 1.09 - 1.13 \rangle)$	T01
sH ₂ O ^{H1}	$\langle 1.60 - 1.70 \rangle - \langle 1.45 - 1.48 \rangle$	$0.5 \times (\langle 1.60 - 1.70 \rangle + \langle 1.45 - 1.48 \rangle)$	T01
sH ₂ O ^{H2}	$\langle 1.60 - 1.70 \rangle - \langle 1.77 - 1.81 \rangle$	$0.5 \times (\langle 1.60 - 1.70 \rangle + \langle 1.77 - 1.81 \rangle)$	T01
sH ₂ O ^K	$\langle 2.12 - 2.16 \rangle - \langle 1.96 - 1.99 \rangle$	$0.5 \times (\langle 2.12 - 2.16 \rangle + \langle 1.96 - 1.99 \rangle)$	T01
H ₂ O ^B	Average of 1.47–1.49	Average of 1.59–1.61	R01
H ₂ O 1.5 μm	Sum of 1.46–1.48	Sum of 1.57–1.59	G02
CH ₄ 2.2 μm	Sum of 2.08–2.12	Sum of 2.215–2.255	G02

1.4.3 Spectroscopy of T dwarfs

T dwarfs or methane dwarfs, objects cooler than L dwarfs, are all brown dwarfs have effective temperatures below 1300 K. Most of them were discovered among the SDSS (Strauss et al. 1999; Tsvetanov et al. 2000; Leggett et al. 2000; Geballe et al. 2002) and the 2MASS (Burgasser et al., 1999, 2000a, 2000b, 2002, 2003b, 2003c) surveys. The remainder were found as companions (Els et al. 2001), in deep fields (Liu et al. 2002b; Cuby et al. 1999), and in proper motion surveys (Scholz et al. 2003; McCaughean et al. 2004). A list of T dwarf discoveries with magnitudes, spectral types, and references is available on Burgasser’s webpage⁴. There are currently 50 T dwarfs known (May 2004).

T dwarfs exhibit very red optical colours, redder than L dwarfs, making them often invisible in the *R* filter and sometimes in the *I* filter. The optical-to-infrared colours are very red ($R-J \geq 9.0$; Golimowski et al. 1998) with an increase towards later types.

Contrary to the optical colours, however, the infrared colours are bluer than L dwarfs and decrease towards later types due to:

- Methane absorption in the *H* and *K* bands
- Strong water vapour bands depressing the flux in the *K* band
- H₂ pressure-induced absorption lines increasing the opacity longwards of 2.0 μm

Infrared colours of T dwarfs are provided here as an indication: $-0.5 \leq J-H \leq 0.9$, $-0.9 \leq J-K \leq 1.4$, and $1.5 \leq K-L' \leq 2.5$. A large scatter is observed in infrared colours particularly towards

⁴<http://www.astro.ucla.edu/~adam/homepage/research/tdwarf>

later types (Hawley et al. 2002). Furthermore, colours and magnitudes are strongly dependent on the filter systems used, with variations up to 30 % (Hawley et al. 2002; Stephens & Leggett 2004). A transformation between filter systems is required prior to any comparison.

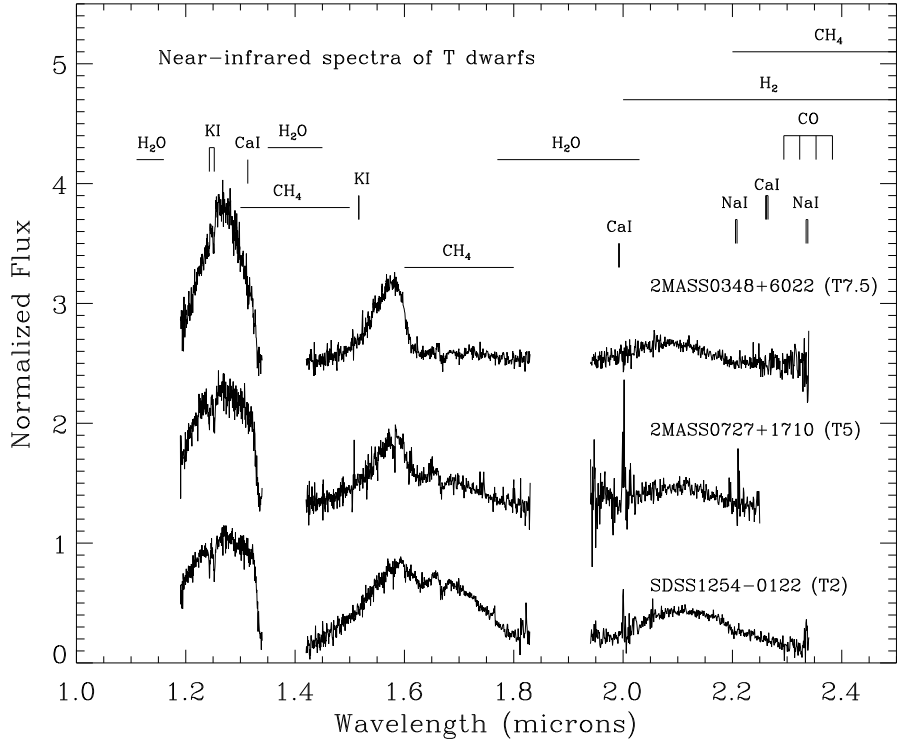


Figure 1.5: Examples of near-infrared ($1.0\text{--}2.5\,\mu\text{m}$) spectra of T dwarfs along with the main molecular features and atomic lines. From top to bottom, the T dwarfs are 2MASS0348+6022 (T7.5; Burgasser et al. 2003c) 2MASS0727+1710 (T5; Burgasser et al. 2002), and SDSS1254–0122 (T2; Burgasser et al. 2002). Near-infrared spectra, available on Burgasser’s webpage, are normalised at $1.28\,\mu\text{m}$ and offset for clarity.

Optical spectra of T dwarfs exhibit less striking features than M and L dwarfs. Pressure-broadened Na I at $5890/5895\,\text{\AA}$ and K I at $7665/7699\,\text{\AA}$ resonance doublets are responsible for the shape of T dwarf shortwards of $8000\,\text{\AA}$. Strong neutral alkali absorption lines of Cs I (8521 and $8943\,\text{\AA}$) and Rb I (7800 and $7948\,\text{\AA}$) and strong H₂O band at $9250\,\text{\AA}$ are present as well. Metallic hydrides such as FeH at $8692\,\text{\AA}$ and CrH at $8611\,\text{\AA}$ and $9969\,\text{\AA}$ are present in early-T dwarfs and vanish at mid-T.

Contrary to L dwarfs, no accurate optical classification scheme is available for T dwarfs due to their faintness at those wavelengths and their red colours. Optical spectra, even obtained with the largest telescopes, are often noisy, hampering the definition of spectral indices.

Near-infrared spectra (Figure 1.5) are mostly shaped by strong water ($1.11\text{--}1.6\,\mu\text{m}$, $1.35\text{--}1.45\,\mu\text{m}$, and $1.77\text{--}2.03\,\mu\text{m}$) and methane ($1.30\text{--}1.50\,\mu\text{m}$, $1.60\text{--}1.80\,\mu\text{m}$, and $2.20\text{--}2.50\,\mu\text{m}$) bands.

Strong KI doublets at 1.17, 1.25, and 1.45 μm as well as the NaI doublet at 2.21 μm are also present. The CO band at 2.3 μm is detected in early T dwarfs but disappear at later types. Finer features of the metallic hydride FeH are seen at 1.19, 1.21, and 1.237 μm . Finally, the collision-induced H₂ exhibit no distinct band head but suppresses the flux longwards of 2.0 μm . Methane and carbon monoxide have been detected at 3.3 μm and 4.7 μm in L dwarfs and in Gl229B, respectively (Noll et al. 1997) and are attributed to vertical mixing in the upper atmospheres (Saumon et al. 2000).

Table 1.4: Near-infrared spectral indices for the classification of T dwarfs as defined by Burgasser et al. (2002; B02) and Geballe et al. (2002; G02).

Index	Numerator (μm)	Denominator (μm)	Feature	Ref
H ₂ O-A	Average of F _{1.12–1.17}	Average of F _{1.25–1.28}	1.15 μm H ₂ O/CH ₄	B02
H ₂ O 1.2 μm	Sum of F _{1.26–1.29}	Sum of F _{1.13–1.16}	1.12 μm H ₂ O	G02
H ₂ O-B	Average of F _{1.505–1.525}	Average of F _{1.575–1.595}	1.4 μm H ₂ O	B02
H ₂ O 1.5 μm	Sum of F _{1.57–1.59}	Sum of F _{1.46–1.48}	1.5 μm H ₂ O	G02
H ₂ O-C	Average of F _{2.00–2.04}	Average of F _{2.09–2.13}	1.9 μm H ₂ O	B02
H ₂ O 2.0 μm	Average of F _{2.09–2.11}	Average of F _{1.975–1.995}	1.9 μm H ₂ O	B02
CH ₄ -A	Average of F _{1.295–1.325}	Average of F _{1.25–1.28}	1.3 μm CH ₄	B02
CH ₄ -B	Average of F _{1.64–1.70}	Average of F _{1.575–1.595}	1.6 μm CH ₄	B02
CH ₄ 1.6 μm	Sum of F _{1.56–1.60}	Sum of F _{1.635–1.675}	1.6 μm CH ₄	G02
CH ₄ -C	Average of F _{2.225–2.275}	Average of F _{2.09–2.13}	2.2 μm CH ₄	B02
CH ₄ 2.2 μm	Sum of F _{2.08–2.12}	Sum of F _{2.215–2.255}	2.2 μm CH ₄	G02
H/J	Average of F _{1.50–1.75}	Average of F _{1.20–1.325}	NIR colour	B02
K/J	Average of F _{2.00–2.30}	Average of F _{1.20–1.325}	NIR colour	B02
K/H	Average of F _{2.00–2.30}	Average of F _{1.50–1.75}	NIR colour	B02
CO	Average of F _{2.325–2.375}	Average of F _{2.09–2.13}	2.3 μm CO	B02

Two near-infrared classification schemes have been proposed by Burgasser et al. (2002) and Geballe et al. (2002) based on the 2MASS and SDSS samples, respectively. The near-infrared classification schemes of T dwarfs are generally more accurate than for L dwarfs due to much wider observed ranges in spectral indices. To first order, T dwarfs can be classified by direct inspection, noting the strengthening of methane absorption at 1.6–1.7 μm and 2.2 μm towards later types.

To quantify the classification, Burgasser et al. (2002) defined several indices (Table 1.4) to measure the strength of water, methane and carbon monoxide features. These regions have been chosen to sample the peak of the *J*, *H*, and *K* broad-band filters and the associated pseudo-continuum. Additional spectral indices have been defined to probe the near-infrared colours at 1.25, 1.6, and 2.1 μm .

Geballe et al. (2002) independently proposed three water spectral indices at 1.2, 1.5, and 2.0 μm and two methane spectral indices at 1.6 and 2.2 μm (Table 1.4). The advantage of Geballe et al. (2002) classification is the extension towards L dwarfs. For example, the water index at 1.5 μm and the methane index at 2.2 μm are sufficiently monotonic through the L-T sequences to classify both types of objects.

The recipe to classify T dwarfs consists of measuring all indices listed in Table 1.4 and then comparing the results to the standard values given in Burgasser et al. (2002) and Geballe et al. (2002). After rejecting the lowest and highest results, the values are averaged, yielding spectral

types accurate to half a subclass or better. Additional measurements of template T dwarfs observed with the same instrument setup as the science target would refine the spectral classification.

A project is underway for a joint classification scheme in the spirit of the MK scheme. The main goals are the following (Burgasser et al. 2003a):

- Define T dwarf standards for each subclass from T0 to T8. These standards must be single, bright, and accessible from both hemispheres.
- Obtain uniform spectral coverage for each standard.
- Define optimal spectral indices, useful over broad range of resolution that avoid contaminating telluric absorption features.

Analysis of the gravity-dependence of spectral features, including collision-induced H₂, is a future goal to allow differentiation between young and old T dwarfs to the field and in open clusters, respectively.

1.5 Different kinds of searches for brown dwarfs

The theoretical prediction of the existence of objects unable to fuse hydrogen in their cores led astronomers to improve their search methods and probe the sky at greater depths.

The advent of infrared detectors, wide-field capabilities at optical and infrared wavelengths and adaptive optics facilities has triggered discoveries of numerous brown dwarfs in various environments. Discoveries of brown dwarfs as companions to solar-like stars, low-mass stars, and substellar objects are reported in § 1.5.1. Large-scale and proper motion survey contributions are presented in § 1.5.2. Searches for young brown dwarfs in star-forming regions and in open clusters are highlighted in § 1.5.3 and in § 1.5.4, respectively.

1.5.1 Brown dwarfs as companions

The confirmation of brown dwarfs is mostly based on the detection of the lithium absorption line at 6708 Å, on the low-luminosities and cool temperatures. To date, no direct dynamical mass measurement of a brown dwarf has been reported. The observation of a full orbit of the low-mass binary Gl569Bab with adaptive optics by Lane et al. (2001) provided an accurate estimate of the total mass of the system. The secondary is incontrovertibly substellar whereas the primary is either a low-mass star or a brown dwarf depending on the age. The detection of brown dwarfs as companions to stars and brown dwarfs is of prime importance to investigate several aspects of star formation, including:

1. Mass ratios provide a constraint to the formation mechanism(s) of low-mass stars and brown dwarfs
2. Correct the Initial Mass Function for binarity.
3. Study the binary frequency as a function of mass in the field and in open clusters
4. Dynamical masses would allow us to test evolutionary tracks at different ages

A variety of surveys have been undertaken to unveil brown dwarfs around objects covering a large range in mass from solar-type stars to the recently defined T class. Different methods are employed to probe certain zones around field dwarfs. The close orbits within few astronomical units are the realms of radial velocity searches. Separations of 1 to 10 AU are probed by speckle imaging. Coronagraphic surveys are best suited to investigate companions with separations between 10 and 100 AU. Wider companions (> 100 AU) are most efficiently searched with wide-field surveys. This section summarises the current knowledge of the frequency of brown dwarf companions to solar-type stars and low-mass stars.

Radial velocity surveys

The presence of a companion around a star can be inferred by the perturbation it engenders in the radial velocity of the star. This constitutes the hallmark of the radial velocity surveys started about 25 years ago to unveil extrasolar planets around solar analogues.

The first extrasolar planet was discovered a pulsar by Wolszczan & Frail (1992). The first extrasolar planet orbiting a solar-type star was discovered around 51 Peg by Mayor & Queloz (1995), the same year as the first unambiguous brown dwarfs. Prior to this discovery, planetary companions were detected around the pulsars PSR1829–10 (Bailes et al. 1991) and PSR1257+12 (Wolszczan & Frail 1992). Hundreds of F, G, K, and M dwarfs have now been surveyed by radial velocity programs with sensitivities reaching few metres per seconds (Mayor et al. 1992; Marcy & Butler 1992; McMillan et al. 1994; Cochran & Hatzes 1994).

To date, more than hundred extrasolar planets have been uncovered by Doppler measurements⁵ within 3 AU of their parent stars and masses as low as the mass of Jupiter (Butler et al. 2003). About five percent of the surveyed solar-type stars harbour one or multiple planets with a wide range of eccentricities and periods. The analysis of 164 nearby solar-type stars by Duquennoy & Mayor (1991) indicates that about 13 % of G dwarfs have stellar companions within the same separation limit.

The distribution of masses of extrasolar planets around solar like stars is peaked at low masses ($1\text{--}2 M_{\text{Jup}}$) with a decreasing power law towards larger masses (see Figure 17 in Vogt et al. 2000 for example). Radial velocity surveys are *not* biased against the discovery of brown dwarfs (defined here as object more massive than $13 M_{\text{Jup}}$) as their perturbation on the parent stars is stronger than planets. This observed lack of brown dwarf companions at low separation around solar-type stars is suggestive of the existence of a “brown dwarf desert”. The $\sin i$ uncertainty on the measurement of the mass does not affect the shape of the distribution of objects as a function of mass because the probability to see a brown dwarf at small inclination is negligible, according to numerous simulations (Queloz 2002).

A radial velocity survey of about 1000 stars with a precision of 0.5 km s^{-1} implemented by Latham et al. (1989) announced the first brown dwarf candidate among 20 radial velocity standards. The object, HD114762, stood out of the sample with a lower limit of 11 Jupiter masses. The current status of this object remain controversial due to the uncertainties on the inclination (Halbwachs et al. 2000).

To date, a dozen brown dwarf candidates extracted from radial velocity programs have been reported. Mayor et al. (1992) found nine stars with possible substellar companions from a survey of 540 nearby F and G dwarfs. Mazeh et al. (1996) investigated low-amplitude radial velocity

⁵<http://www.obspm.fr/encycl/cat1.html>

variations of three stars belonging to the original list of radial velocity standards. Tokovinin et al. (1994) merged radial velocity observations accomplished independently with two spectrometers to infer a mass of $60 M_{Jup}$ for one companion. However, the orbital inclinations from the *Hipparcos* satellite concluded that most of them are simply stellar companions (Halbwachs et al. 2000). Seven objects are definitely rejected as brown dwarf companions, one is accepted with a low confidence level, and the remainder require additional studies to assess their substellarity.

Three additional brown dwarfs, with masses ($m \sin i$) ranging from 13 to $18 M_{Jup}$, have been reported around HD168443 (Marcy et al. 1999), HD162020, and HD202206 (Udry et al. 2002). These three candidates remain, to date, the sole bona-fide substellar companions found by Doppler measurements. It is worth mentioning that HD168443 is a system composed of an extrasolar planet/brown dwarf pair orbiting the nearby high proper motion K dwarf, Gl 86A (Els et al. 2001).

To summarise, the present set of data drawn from radial velocity surveys indicates that less than 0.5 % of solar-type stars harbour close brown dwarf companions (Marcy & Butler 2000; Zucker & Mazeh 2001). The extension of this brown dwarf desert at wide separation is ruled out by current observations, suggesting a frequency comparable to stellar companions despite the large uncertainties ($18 \pm 14\%$; Gizis et al. 2001a).

Microlensing

The main principle of microlensing, originally suggested by Paczynski (1986), is the following: when the “lens” is aligned with a distant bright star, it bends and distorts the light of the background object, yielding an enhancement of flux on a short timescale. Several types of lenses are possible, including compacts objects in external galaxies or disk objects in our Galaxy such as normal stars, brown dwarfs and planets.

Various collaborative efforts are under way to unveil extrasolar planets and brown dwarfs. Among them are the MACHO project, the Optical Gravitational Lensing Experiment (OGLE), the Expérience pour la Recherche d’Objets Sombres (EROS), Microlensing Observations in Astrophysics (MOA), Microlensing Follow-up Network (MicroFUN), the Microlensing Planet Search (MPS), and Probing Lensing Anomalies Network (PLANET).

The search for brown dwarfs through microlensing is just starting. Three possible candidates have been recently reported but the uncertainties on the mass determination remain large and additional observations are obviously required to further constrain the nature of the lens.

1. Alcock et al. (2001) observed a microlensing event in the Large Magellanic Clouds with the *Hubble Space Telescope*, yielding a mass estimate between 0.03 and $0.10 M_{\odot}$. Optical spectroscopy of the lens suggests however a mass larger than $0.09 M_{\odot}$, placing the object above the hydrogen-burning limit.
2. Smith et al. (2003) inferred a mass of $M \sim 0.050^{+0.016}_{-0.011} M_{\odot}$ for a bright microlensing event observed towards the Galactic bulge by the OGLE project. If verified, the lens would be a brown dwarf located at a distance of 6.5 kpc.
3. A recent microlensing event toward M31 was announced by An et al. (2004). The lens is a binary system located either in the disk of M31 or in the halos of the Milky Way or M31. The secondary is either a brown dwarf or a low-mass star depending on the distance of the system.

Brown dwarf companions to low-mass stars

The first brown dwarf companion candidate was found around a white dwarf, GD165 (Becklin & Zuckerman 1988). This object is now recognised as a template for the newly-defined L class and is likely a brown dwarf (Kirkpatrick et al. 1999a). The first T dwarf, Gl229B, was discovered orbiting an early-M dwarf (Nakajima et al. 1995). Those discoveries have triggered a large number of high-resolution imaging surveys conducted with the *Hubble Space Telescope* and adaptive optics systems on the world's largest telescopes to uncover new brown dwarf companions to low-mass stars. A brief overview is provided below and in Table 1.5.

The most complete population available to date to investigate the binary frequency of low-mass stellar and substellar companions are the 5- and 8-pc samples. Several programs have been dedicated to the closest neighbours to the Sun to unveil companions over different separation ranges. Henry & McCarthy (1990) failed to detect new brown dwarfs at separations closer than 10 AU from a systematic search around M dwarfs within 5 parsecs using infrared speckle interferometry. Simons, Henry, & Kirkpatrick (1996) investigated separations between 100 and 1400 AU around 63 systems within 8 pc and $\delta \geq -25^\circ$. Second-epoch observations supplemented the previous search with proper motion as primary criterion but did not uncover new low-mass companions (Hinz et al. 2002). High-resolution imaging of 23 nearby dwarfs within 13 pc carried out with the *Hubble Space Telescope* failed to detect any companion at separations between 1 and 50 AU (Schroeder et al. 2000). Similarly, a coronagraphic survey of 107 nearby star systems probing separations ranging from 40 to 100 AU turned up no new brown dwarf companions (Oppenheimer et al. 2001). It sounds likely that all stellar companions to nearby dwarfs have now been detected by the extensive programs implemented over several decades (Reid & Gizis 1997a).

New low-mass stars and brown dwarf companions have been detected around K (Gizis, Kirkpatrick, & Wilson 2001b), G (Potter et al. 2002; Goto et al. 2002; Liu et al. 2002a), M (Rebolo et al. 1998; Goldman et al. 1999; Martín et al. 2000b; Lane et al. 2001; Close et al. 2002a; Freed et al. 2003), and L dwarfs (Martín et al. 1999a; Koerner et al. 1999). Table 1.5 lists those discoveries along with their parameters, including spectral types of the primary and secondary (when a spectrum was obtained), distance and age of the system, as well as the separation in astronomical units. The secondary of these systems is either a low-mass star or a brown dwarf depending on the age of the system. The separation and mass ratio distributions of ultracool dwarfs are plotted in Figure 1.6.

Large samples of ultracool dwarfs with spectral types ranging from M8 to T8 have been recently implemented to improve statistics in order to investigate the binary frequency of substellar mass objects to very low-mass stars and brown dwarfs.

Reid et al. (2001b) reported the discovery of four binary systems out of 20 L dwarfs observed with the *Hubble Space Telescope*. The low-mass binaries have separations spanning 2–8 AU with near equal-masses. However, one object did exhibit a much fainter companion, suggesting a mass ratio (q_1/q_2) as low as 0.8.

A sample of 10 T dwarfs observed by Burgasser et al. (2003b) unveiled two binary systems. As for the previous study by Reid et al. (2001b), both systems are tight binaries within 4 AU with near equal-brightness ratios.

A survey of 39 late-M dwarfs with spectral types later than M8 revealed nine binary systems (Close et al. 2002a, 2002b, 2003). The large majority of primaries are low-mass stars with spectral types M8–L0.5 and the secondaries are either stellar or substellar depending on the and distance.

Table 1.5: List of low-mass stellar and brown dwarf companions to stars. Note that Gl569B and HD130948 orbit normal stars and were resolved as binary systems. The remaining low-mass stellar and brown dwarf companions to ultracool dwarfs found in the course of recent high-resolution imaging surveys (Reid et al. 2001b; Close et al. 2002b; Burgasser et al. 2003b; Gizis et al. 2003; Close et al. 2003; Bouy et al. 2003) are given in Table 4 in Close et al. (2003) with their estimated parameters (separation, spectral types, masses and periods).

References: (1) Rebolo et al. 1998 (2) Martín et al. 1999a (3) Goldman et al. 1999 (4) Martín et al. 2000b (5) Burgasser et al. 2000a (6) Lane et al. 2001 (7) Gizis et al. 2001b (8) Potter et al. 2002 (9) Goto et al. 2002 (10) Liu et al. 2002a (11) Close et al. 2002a (12) Freed et al. 2003.

Name	SpT Primary	Distance pc	Age system Gyr	Separation AU	Characteristics Secondary	Refs
G196-3	M2.5	21	~ 0.1	~ 300	BD Lithium	1
LHS102	M3.5	9.6	~ 1	~ 200	BD or VLM	3
Gl569ABa/Bb	M2	9.8	< 1	50 and 1	M8.5/M9.0	4,6
GD570ABCD	K4	5.9	2–10	1525	T8; BD	5
GJ1048	K2	21.2	≤ 1	250	L1	7
HD130948ABa/Bb	G2	18	< 0.8	50 and 2.4	L2–L4/L2–L4	8,9
15 Sge	G1	17.7	1–3	14	L2–L6	10
2MASS J1426316+155701	M8.5	18.8	0.5–7.5	2.92	L1–L3	11
LHS2397a	M8	14.3	2–12	2.96	L7.5	12

The main conclusions are similar to previous surveys. Two systems exhibit, however, fainter companions suggestive of low-mass ratios (e.g. Freed et al. 2003).

The largest sample of ultracool dwarfs studied to date explored 134 objects (Bouy et al. 2003), including 20 L dwarfs (Reid et al. 2001b), 84 M and L dwarfs (Gizis et al. 2003), and 30 new objects. Except one target associated with a G dwarf in a triple system, 25 out of the 133 ultracool dwarfs turned out to be binaries. This statistically significant study suggests a binary fraction around 10 % among field dwarfs within 25 pc. The main conclusions drawn by these recent surveys are discussed in the conclusions of this section.

Brown dwarf binaries

Brown dwarf binaries are of prime importance to test evolutionary tracks in the substellar regime. Close binaries are most suitable to obtain dynamical masses over a short timescale. However, the number of known field brown dwarf binaries is low and most of them do not have a resolved spectrum. Note that PPI15 is the only spectroscopic binary (Basri & Martín 1999b) and is a member of the Pleiades open cluster.

All genuine brown dwarf binaries discovered to date are listed in Table 1.6 along with their estimated physical parameters, including distances, spectral types, separation, mass ratio, and period. Only three systems have accurate distances, namely 2MASSW 1146345+223053, DENIS-PJ 0205.4–1159, and ε Indi B.

Few other objects are suggested as possible binary brown dwarfs, including Gl569Ba/Bb (Martín et al. 2000b; Kenworthy et al. 2001; Lane et al. 2001), HD130948B/C (Potter et al. 2002;

Table 1.6: List of brown dwarf binaries discovered to date in the field and in the Pleiades along with the estimated physical parameters. The distance of the system is given in parsecs, the separation in astronomical units (AU), the spectral types, the mass ratio (q parameter), and the period in years.

References: (1) Martín et al. 1999a (2) Koerner et al. 1999 (3) Reid et al. 2001b (4) Burgasser et al. 2003b (5) Gizis et al. 2003 (6) Bouy et al. 2003 (7) McCaughrean et al. 2004. (8) Martín et al. 2003.

Name	Distance pc	Sep AU	SpT	Mass ratio q	Period yr	Refs
2MASSs 0850359+105716	27.7	4.4	L6/??	0.75	43	3,6
2MASSW 0920122+351742	20.8	1.6	L6.5/??	1.0	16	3,6
2MASSW 1146345+223053	26.2	7.6	L3/??	1.0	70	2,3
2MASS 1225–2739AB	11.2	3.0	T6/T8	0.7–0.8	25–40	4
2MASS1239272+551537	21.3	4.0	L5/L5	1.0	30	5,6
2MASS 1534–2952AB	16.5	1.0	T5/T5	1.0	4–6.5	4
2MASS1728114+394859	20.4	3.4	L7/early T	0.8	30	5,6
2MASS2101154+175658	23.2	4.0	L7.5/L8	1.0	42	5,6
DENIS-PJ 0205.4–1159	18.0	9.2	L7/L7	1.0	??	2
DENIS-PJ 1228.2–1547	18.1	5.0	L5/??	1.0	35	1,2
ε Indi B	3.626	2.65	T1/T6	0.6	15	7
CFHT-PI-12	125	7.75	—	0.7	76	8
IPMBD25	125	11.75	—	0.62	126	8
IPMBD29	125	7.25	—	0.84	68	8

Goto et al. 2002), 2MASSW 0746425+200032 (Reid et al. 2001b), and 2MASS1426316+155701 (Close et al. 2002a). The masses remain uncertain due to the lack of lithium in absorption and uncertainties on the age and/or distance. As a consequence, the primary is a very low-mass star or a brown dwarf and the secondary a brown dwarf.

Conclusions to the frequency of brown dwarfs as companions

The main results of programs dedicated to the search for substellar companions to very low-mass stars and brown dwarfs can be summarised as follows:

1. A few brown dwarf companions have been detected within 3 AU around main-sequence stars by radial velocity surveys, yielding a binary frequency less than 0.5 % and suggestive of a “brown desert” at these separations. A dearth of brown dwarfs at wide separations (> 1000 AU) is not apparent around main-sequence (F–M0) stars (Gizis et al. 2001a) with a frequency of 18 ± 14 %. Studies dedicated to intermediate separations are barely under way. The binary frequency of ultracool field dwarfs lies around 10–15 % in contrast with 57 ± 9 % for G dwarfs (Duquennoy & Mayor 1991) and 42 ± 9 % for M dwarfs (Fischer & Marcy 1992). The frequency of binary brown dwarfs of at most 5 % predicted by recent simulations (Bate et al. 2002; Delgado-Donate et al. 2003) is lower than the observed values.
2. Very low-mass and brown dwarf binaries have separations smaller than 16 AU with a peak in the distribution occurring around 4–8 AU (Left panel in Figure 1.6). Similarly, surveys in the Hyades (Reid & Gizis 1997b) and in the Pleiades (Martín et al. 2000a) produced no

brown dwarf companions with separations larger than 14 and 27 AU, respectively. These results are at odds with the distribution of companions around M dwarfs. Firstly, about 40 % of M dwarf multiple systems within 8 pc have separations greater than 10 AU (Reid & Gizis 1997a). Secondly, 50 % of M0–M6 dwarfs have separations between 10 and 10^4 AU (Fischer & Marcy 1992). Furthermore, the distribution of separation of G and M dwarfs is much broader with a maximum from 3 to 30 AU (Fischer & Marcy 1992; Duquennoy & Mayor 1991). Current techniques are sensitive to wide low-mass stellar and substellar companions but suffer from observational biases towards spectroscopic binaries.

3. Low-mass binaries in the field tend to favour equal-mass systems with mass ratios larger than 0.8 (Right panel in Figure 1.6). The lowest mass ratio is the ε Indi B system with $q \sim 0.6$ (McCaughrean et al. 2004). This might simply reflect the lack of sensitivity to companions fainter than the primary by more than 4 mag. These results are in agreement with the peak at equal-mass systems noticed in the 8-pc sample (Reid & Gizis 1997a) but are at odds with the flatter distributions of G dwarfs which peaks around $q = 0.2$ (Duquennoy & Mayor 1991). Dynamical simulations of small clusters predict a flat mass ratio distribution of brown dwarfs with a rarity of extreme ratios (Delgado-Donate et al. 2003; Sterzik & Durisen 2003) in agreement with current observations.

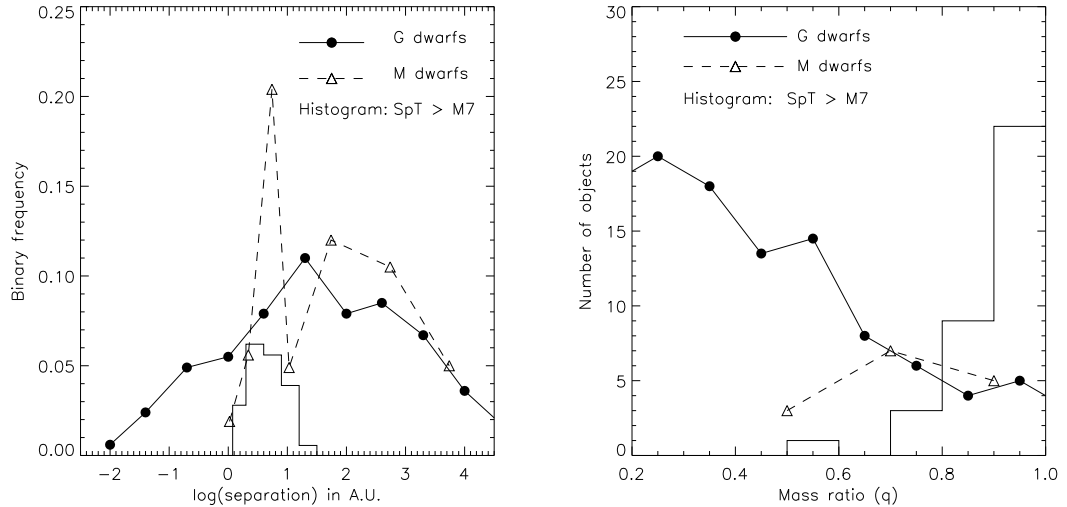


Figure 1.6: Distribution of separation (left panel) and mass ratio (right panel) for G dwarfs (solid line; Duquennoy & Mayor 1991), M dwarfs (dashed line; Fischer & Marcy 1992), and ultracool dwarfs (histogram; see text for all references). We have found a total of 34 binary systems out of 178 ultracool field dwarfs observed with high-resolution imaging from the ground and from space. The binaries found in the Pleiades by Martín et al. (2003) are not plotted as they represent a younger subsample. The errors on the measurements are Poisson errors (not included).

1.5.2 The field brown dwarfs

Over 250 L dwarfs and about 50 T dwarfs have been discovered in the field over the last five years, most of them by three large-area sky surveys, namely the Two Micron All-Sky Survey (hereafter 2MASS), the DEep Near-Infrared Survey (hereafter DENIS), and the Sloan Digital Sky Survey (hereafter SDSS).

The 2MASS (§ 1.5.2), DENIS (§ 1.5.2), and SDSS (§ 1.5.2) surveys, their selection criteria to unearth new L and T dwarfs, and their main discoveries are described. Proper motion surveys aiming at finding ultracool dwarfs in the solar neighbourhood are highlighted in § 1.5.2. Finally, some serendipitous discoveries of L and T dwarfs are presented in § 1.5.2.

The Two Micron All-Sky Survey

The Two Micron All-Sky Survey (<http://ipac.caltech.edu>), project led by the University of Massachusetts, provides full sky coverage in the near-infrared J (1.25 μm), H (1.65 μm), and K_s (2.15 μm) broad-band filters (Skrutskie et al. 1997). The survey was conducted with twin 1.3-m telescopes each equipped with a three-channel 256 \times 256 pixel NICMOS3 camera observing simultaneously in J , H , and K_s . The pixel scale was 2'', yielding a 8.5' \times 8.5' field-of-view. Six frames of 1.3 seconds each were obtained for each individual field on the sky, yielding a total integration time of 7.8 seconds. The nominal survey completeness limit was $J = 15.8$, $H = 15.1$, $K_s = 14.3$ with signal-to-noise of 10 at high galactic latitudes.

The selection method to find nearby L dwarfs was rather crude but highly efficient. All candidates with $J - K_s$ colour redder than 1.2 mag were followed-up spectroscopically with the Keck/LRIS spectrograph to ensure sufficient signal-to-noise. Over 150 nearby L dwarfs were found in the 2MASS database (Kirkpatrick et al. 1999b; Kirkpatrick et al. 2000; Cruz et al. 2003), yielding accurate spectral type classification at optical wavelengths shortwards of 1 μm (Kirkpatrick et al. 1999b).

The CorMASS project aims at low-resolution ($R \sim 300$) spectroscopy of all red ($J - K_s \geq 1.2$) and bright ($K_s \leq 13.0$) to extend the optical classification scheme to the near-infrared (Wilson et al. 2003).

About half of the T dwarfs were discovered in the 2MASS database (Burgasser et al. 1999, 2000a, 2000b, 2002, 2003b, 2003c). Several colour cuts, including $J \leq 16.0$, $J - H \leq 0.4$, and $H - K_s \leq 0.3$ or $J \leq 16.0$, $J - H \leq 0.4$, and $H - K_s \geq 0.3$ were applied to find field T dwarfs in the 2MASS database. Targets were selected to have galactic latitudes above 15° and to avoid the Magellanic Cloud and 47 Tuc regions. Proper motions and optical counterparts present in the Digital Sky Surveys were removed from the initial sample, yielding a small pool of bona-fide T dwarf candidates for near-infrared spectroscopic follow-up.

The 2MASS project is a powerful tool to detect brown dwarfs in the field as well as in open clusters. Several studies made use of the 2MASS database to confirm membership status of cluster candidates in the Pleiades (Tej et al. 2002), in Taurus (Briceño et al. 2002), in MBM12 (Luhman 2001), in α Per (Barrado y Navascués et al. 2002) and to study disk fractions in star-forming regions, including σ Ori (Oliveira et al. 2002).

On the theoretical side, the 2MASS database was used to refine atmosphere models and derive effective temperature scales for ultracool dwarfs (Schweitzer et al. 2001).

The DEep Near-Infrared Survey

The DEep Near-Infrared Survey (<http://www-denis.iap.fr/>) was conducted with the ESO 1-m telescope at La Silla with a three-channel camera in the Gunn-*I* (0.82 μm), *J* (1.25 μm), *K_s* (2.15 μm) filters, covering the whole Southern Sky from -90° to $+2.5^\circ$ (Epchtein et al. 1997). Two NICMOS3 arrays with 256×256 pixels and a pixel size of $3''$ were used in the *J* and *K_s* channels whereas a 1024×1024 Tektronix CCD detector with $1''$ pixel scale was used for the *I* channel. The resulting field-of-view was $12'$. The sky was scanned in step and stare mode along 30 degree strips at constant right ascension with integration time of 10 seconds. The approximate 3σ limits of the survey were $I = 18.5$, $J = 16.5$, $K_s = 13.5$.

The selection criterion to find low-luminosity objects in the field was two-fold (Delfosse et al. 1997, 1999):

- Objects redder than $I-J$ colour of 2.5 mag.
- Objects with *J* and *K* detections and no optical counterpart.

No systematic spectroscopic follow-up was implemented as for 2MASS, yielding a smaller number of L dwarf discoveries. Nonetheless, the DENIS “Mini-Survey” revealed about 20 objects later than M8, including 3 L dwarfs (Delfosse et al. 1999), with optical and near-infrared spectroscopic assessment (Tinney et al. 1998; Delfosse et al. 1999). High-resolution spectroscopy of the 3 L dwarfs placed one object, DENIS-PJ 1228.2–1547, as the first discovered field brown dwarf with Kelu 1 (Ruiz et al. 1997), after detection of lithium absorption at 6708 Å (Martín et al. 1997; Tinney et al. 1997).

The Sloan Digital Sky Survey

The Sloan Digital Sky Survey (<http://sdss.org>) has surveyed over 10000 deg^2 (one fourth of the celestial sphere) of the high galactic latitude sky, centred approximatively on the North Galactic Pole, with a dedicated 2.5-m telescope at the Apache Point Observatory (York et al. 2000). The SDSS project imaged the sky in 5 filters (*u*, *g*, *r*, *i*, and *z*), covering the 0.4 – $1.0 \mu\text{m}$ wavelength range (Fukugita et al. 1996).

The imaging array was a mosaic of thirty 2048×2048 CCDs with $0.396''/\text{pix}$ providing a total field-of-view of $2.5^\circ \times 13'$. The effective integration time was 54.1 seconds per filters per print on sky. The expected completeness limits (5σ detection limit) of the survey were $u \sim 22.3$, $g \sim 23.3$, $r \sim 23.1$, $i \sim 22.3$, and $z \sim 20.8$, assuming a full-width-half-maximum of $1''$ and an airmass of 1.4. Photometric calibration was obtained with a small auxiliary telescope at the same site. Different types of objects were followed-up spectroscopically with a dedicated SDSS twin fibre-fed spectrograph. Fibres were $3''$ in diameter and provided wavelength coverage from 3800 to 9200 Å at $R \sim 1800$.

The SDSS commissioning data revealed about 20 L dwarfs reported in Fan et al. (2000) and Schneider et al. (2002). The selection criteria to find L dwarfs in the SDSS survey are:

1. Objects redder than $i-z \geq 1.6$ and $r-i \geq 1.8$.
2. $i-z \geq 1.6$ and 2σ detection in *i* and/or detection in the 2MASS catalogue for objects undetected in the *r* images.

The search for T dwarfs in the SDSS data took into account the faintness and the red optical colours of these objects, considering the following search criteria:

1. Detection above 3σ in i and detection twice in the z filter with 2MASS counterpart.
2. Detection only in the z -band required $z \leq 19.0$.

A dozen T dwarfs were discovered in the SDSS commissioning data (Strauss et al. 1999; Tsvetanov et al. 2000), including the first L/T transition objects (Leggett et al. 2000). Geballe et al. (2002) developed a near-infrared classification scheme for ultracool dwarfs from M to T, according to the SDSS discoveries (Table 1.4).

Proper motion surveys

The knowledge of the solar neighbourhood, defined as the volume of space within 25 pc, was largely established by photographic proper motion surveys prior to the advent of large-area digital sky surveys. Despite the large number of ultracool dwarfs unearthed by the 2MASS, DENIS, and SDSS surveys, the census of the solar vicinity is incomplete at the faint end by 30 % within 10 pc (Henry et al. 1997) and about twice this value within 25 pc (Henry et al. 2002). Trigonometric parallaxes represent the best way to measure distances but proper motions remain a good distance discriminant when the spectral type of the object is known.

The most extensive proper motion databases available to date are two catalogues compiled by Luyten based mainly on data obtained with the 1.2-m Palomar Oschin Schmidt telescope and published more than twenty years ago:

1. The Luyten Catalogue of Stars with Proper Motions Exceeding $0.5''/\text{yr}$ Annually (hereafter LHS; Luyten 1979) lists about 3600 stars with $\mu \geq 0.500''/\text{yr}$ and hundreds of stars with proper motions spanning $0.235\text{--}0.500''/\text{yr}$.
2. The New Luyten Catalogue of Stars with Proper Motions larger than Two-Tenths of an Arcsecond (hereafter NLTT; Luyten 1980) represents a compilation of 58,845 stars with proper motions larger than $0.18''/\text{yr}$.

Two epochs were obtained with positions accurate to a few arcseconds. Magnitudes measured in two photographic passbands m_{pg} and m_r , corresponding roughly to the current photometric B and R_{Kron} , respectively, were accurate to about 0.5 mag. The faintest stars catalogued have $m_r \sim 19$ and $m_{pg} \sim 20.5$, respectively.

South of $\delta \leq -33^\circ$, both the LHS and the NLTT catalogues were extended using data from the Bruce Proper Motion survey conducted with the 0.65-m Bruce refractor beginning of the 20th century. Although the Bruce survey extended to proper motions down to $0.1''/\text{yr}$, only stars brighter than $m_{pg} \sim 15.5$ were catalogued with a blue magnitude but no colour information. The search for low-luminosity objects in the south is, thus, highly hampered by the bright detection limit of the Bruce catalogue. New faint proper motion objects down to $m_r = 19.5$ and south of $\delta < -5^\circ$ were extracted by Wroblewski & Torres (1989, 1992, 1994, 1995, 1996, 1997, 1998) and Wroblewski & Costa (1999, 2000, 2001).

To improve the census of the solar neighbourhood and characterise the luminosity and mass functions across the stellar/substellar boundary, several proper motion surveys have recently been implemented both in the Northern and Southern hemispheres. We will briefly highlight the results

of the surveys which contributed to the discovery of low-mass stars and brown dwarfs in the solar vicinity, including our own Southern Sky proper motion survey for nearby red dwarfs presented in details in Chapter 2.

- Reid & Cruz (2002), Reid, Kilkenny, & Cruz (2002b), and Cruz & Reid (2002) presented a series of papers aiming at finding low-mass stars and brown dwarfs within 20 pc. By cross-correlating the NLTT catalogue with an early release of the 2MASS database for galactic latitudes higher than 10° , the authors discovered over 100 new ultracool dwarfs based on their location in the $(m_r, m_r - K_s)$ colour-magnitude diagram. Although photometric distances are subject to large uncertainties due to errors on photometric measurements or binarity, these results demonstrate clearly the incompleteness of the solar neighbourhood, especially at the low-luminosity end.

More recently, Cruz et al. (2003) initiated a volume-limited ($d \leq 20$ pc) survey of nearby M7–L6 dwarfs over the whole sky entirely based on the 2MASS survey. Moderate-resolution ($R \sim 3000$) optical (6000–10000 Å) spectroscopy provided spectral types and photometric distances for each individual object, yielding the discovery of 39 new L dwarfs. A bright ($K_s = 9.1$) M8.5 dwarf at 6 pc with a proper motion of $0.759''/\text{yr}$ was uncovered within the framework of this search (Reid et al. 2003).

- Lépine, Shara, & Rich (2002) conducted a systematic search for high proper-motion stars ($0.5 \leq \mu \leq 2.0''/\text{yr}$) at low-galactic latitudes ($|b| \leq 20^\circ$) using the Digital Sky Survey database. The same procedure was recently extended to galactic latitudes above 25° (Lépine, Rich, & Shara 2003a). Most of the high proper motion ($0.5 \leq \mu \leq 2.0''/\text{yr}$) stars listed in Luyten's catalogues were recovered and new objects brighter than 20.0 mag were discovered. The search method was based on the SUPERBLINK software developed by the authors to recover high proper motion stars in an automatic way after scaling, shifting, rotating, and subtracting the POSS I and POSS II photographic plates. This tool was specifically optimised to work on relatively crowded fields and to improve the detection of proper motion stars affected by a bright neighbour.

Optical spectroscopy of numerous new high proper motion stars revealed white dwarfs, M dwarfs, metal-poor dwarfs (Lépine, Rich, & Shara 2003b) as well as:

1. A high proper motion ($\mu = 2.38''/\text{yr}$) faint ($V = 19.3$) M8.5 dwarf at 14 pc (Lépine, Shara, & Rich 2002).
 2. A bright ($K_s \sim 10.9$) L1 brown dwarf at 10 pc confirmed by the detection of lithium at 6708 Å (Salim et al. 2003).
 3. An early-L subdwarf (Lépine, Rich, & Shara 2003a).
- The Calán-ESO Proper Motion Catalogue contains 542 stars with proper motions larger than $0.2''/\text{yr}$ identified on $5^\circ \times 5^\circ$ ESO red plates taken ~ 10 yr apart (Ruiz et al. 2001). The field selection was random but avoided the high galactic latitude regions with declinations ranging from $\delta = -40^\circ$ to $\delta = -25^\circ$. The two hours integration time yielded photographic magnitudes m_r spanning 7.5–19.5 mag. This proper motion survey, originally aiming at the identification of cool white dwarfs in the solar neighbourhood, led to the discovery of the first field brown dwarf, Kelu-1 (Ruiz, Leggett, & Allard 1997).
 - The Liverpool-Edinburgh catalogue (Pokorny, Jones, & Hambly 2003) is a compilation of about 6200 stars at the South Galactic Cap, with proper motions exceeding $0.18''/\text{yr}$ and

$R=9.0\text{--}19.5$ mag. Interesting objects were selected from the reduced proper motion and colour-colour diagrams for spectroscopic follow-up observations but no new subdwarfs or brown dwarfs have been announced to date.

- A new high proper motion survey was conducted in the Southern Sky south of $\delta \leq -33^\circ$ based on $6^\circ \times 6^\circ$ photographic plates obtained with the UKST telescope and measurements made with the APM machine at Cambridge (Scholz et al. 2000). The initial search was based on measurements in two passbands (B_J and R) at two epochs separated by ~ 15 years for $\delta \leq -20^\circ$. Typical limiting magnitudes are $B_J \sim 22.5$ and $R \sim 21$, with an uncertainty of ~ 0.25 mag. Search radii of 60 to 90 arcsec were used to recover large proper motions (typically $0.3\text{--}1.0''/\text{yr}$).

The pilot survey (Scholz et al. 2000) extracted about 100 new high proper motion objects down to $R \sim 20.0$ over thousand square degrees between 0^h and 7^h in right ascension and -63° and -32° in declination, respectively. This sample included new white dwarfs as well as K and M dwarfs. This survey was later extended by Scholz using the SuperCOSMOS Sky Survey and 2MASS catalogues over the entire southern sky at four different epochs. The new approach, detailed in Chapter 2, led to the discovery of:

1. Six subdwarfs (Chapter 2).
2. Numerous M dwarfs within 50 parsecs (Chapter 2).
3. Two M dwarfs within 10 parsecs (McCaughrean, Scholz, & Lodieu 2002b).
4. Three ultracool dwarfs (Lodieu, Scholz, & McCaughrean 2002b).
5. The closest binary brown dwarf and brightest T dwarf to the Sun, ε Indi Ba/Bb (Scholz et al. 2003; McCaughrean et al. 2004).

Serendipitous discoveries

Besides the large-scale sky surveys which revealed a large number of ultracool dwarfs and the proper motion surveys dedicated to the search for nearby stars, a small number of L and T dwarfs were unearthed during unrelated surveys. Among them, we would like to emphasise the following discoveries:

- Cuby et al. (1999) reported the discovery of a late-T dwarf in the course of a deep survey carried out with the SofI and SUSI instruments mounted on the NTT. The NTT Deep Field covered an area of $2.3' \times 2.3'$ in the B , V , and r filters down to magnitude limits of 27.2, 27.0, and 26.7, respectively. A $5' \times 5'$ field-of-view was observed as well in the J and K_s filters down to magnitude limits of 24.6 and 22.8, respectively. This new T dwarf has $J = 20.15$ and $K_s = 20.3$ and a low-resolution near-infrared spectrum comparable to Gl229B.
- Liu et al. (2002b) presented the discovery of a faint ($I = 23.6$, $J = 18.2$) T dwarf within the framework of the Institute for Astronomy Deep Survey. This survey used the prime-focus imager Suprime-Cam on the Subaru 8.2-m telescope to cover a total area of 2.5 square degrees in the R , I , and z' filters down to 27.1, 26.5, and 25.5, respectively. Optical and infrared colours with additional near-infrared spectroscopy yielded a spectral type of T3–T4 and a photometric distance of 45 ± 9 pc (Liu et al. 2002b).

- As the result of a spectroscopic search for distant AGB stars, Kendall et al. (2003) announced the discovery of seven unknown L dwarfs. All seven objects were very faint on the I -band photographic plates with magnitudes ranging from 17.0 to 20.0 mag. The objects were assigned spectral types between L0.5 and L5 from direct comparison with template L dwarfs.
- Thorstensen & Kirkpatrick (2003) recently discovered a bright ($K_s = 11.3$) L3.5 dwarf within the framework of a parallax program for a sample of cataclysmic binaries. This new L dwarf, 2MASS J0700+3157, has a well determined parallax of 82 ± 2 mas, and constitutes a new addition to the catalogue of nearby stars (Gliese & Jahreiss 1995). It also represents an important addition to the small sample of L and T dwarfs with accurate distances.

1.5.3 Brown dwarfs in star-forming regions

In § 1.5.2, we have described different kinds of searches dedicated to the improvement of the census of stars and brown dwarfs in the solar neighbourhood. The ultimate goal is to derive the luminosity and mass functions of a volume-limited sample of objects. However, the determination of the field IMF is hampered by major drawbacks, including:

- Parallaxes are required for each individual star to infer their masses. The most reliable mass function estimate is currently available for the 5- and 8-pc samples although the incompleteness might be as high as 30 %, particularly towards low-mass stars (Henry et al. 1997).
- Ages are generally unknown and a mean value of the order of 1 Gyr is assumed for nearby objects to infer the mass. The possible time variations occurring in the star formation rate are lost in this process.
- Large incompleteness exists for high-mass stars because of their rarity in the solar neighbourhood and their short lifetimes.
- The incompleteness towards low-mass stars and brown dwarfs is significant due to their faintness (Henry et al. 1997). The recent discovery of the ε Indi Ba/Bb system at 3.626 pc (Chapter 2) provides one counterexample.

To alleviate many of those issues, several studies have focused on embedded clusters and star-forming regions because they represent an equidistant sample of stars with a similar chemical composition within a limited area on the sky. The advantages (+) and drawbacks (−) compared to the solar vicinity are the following:

- + Very low-mass stars and brown dwarfs are brighter when younger at a given distance, making their detection easier in star-forming regions than in the field (Figure 1.2).
- + Small contamination by field stars and background giants due to the presence of dust and the compactness of embedded clusters.
- + Dynamical evolution is obviously low at young ages although the birth of young clusters might go through phases of violent gas expulsion affecting the shape of the IMF (Kroupa et al. 2001). High-mass stars will not have evolved off the main-sequence yet and low-mass stars are retained within the cluster core. The IMF can, therefore, be derived from high-mass stars down to the deuterium burning limit and below.

- Star-forming regions are heavily embedded in their molecular cloud hampering optical observations.
- Large uncertainties are expected on evolutionary tracks at very young ages due to unknown initial conditions (Baraffe et al. 2002).
- The timescale to form stars represents an appreciable fraction of the cluster age. The star formation process is still on-going so that the mass function is a lower limit of the IMF.

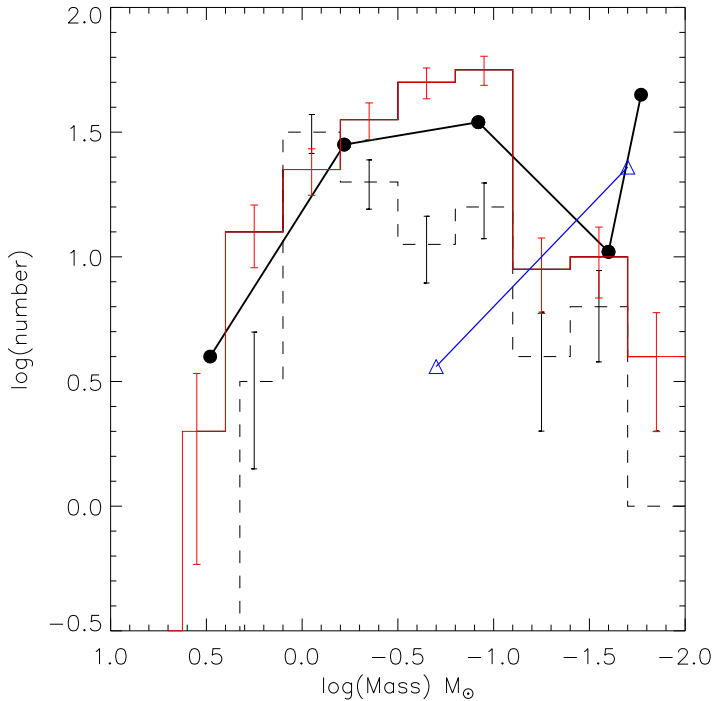


Figure 1.7: Comparison of substellar mass functions in logarithmic scale (Salpeter definition) for the Taurus cloud (dashed histogram; Briceño et al. 2002; Luhman et al. 2003a), the IC348 cluster (solid histogram; Luhman et al. 2003b), the Trapezium Cluster (filled circles with solid line; Muñch et al. 2002), and σ Orionis (open triangles with solid line; Béjar et al. 2001). Possible explanations for the difference in the mass function between Taurus and the Trapezium Cluster are discussed in Section 1.1.3

Bearing in mind those caveats, an emphasis on the recent mass function determinations will follow along with a brief description of the most studied young clusters, including the Trapezium Cluster, σ Orionis, IC348, Taurus, ρ Ophiuchus, and Chameleon (Figure 1.7). Additional star-forming regions have been targeted to uncover low-mass stars and substellar objects but no mass functions were published to date. It includes Lupus (Nakajima et al. 2000), R Corona Australis (Comerón et al. 2002), Upper Scorpius (Martín et al. 2004), NGC1333 (Aspin et al. 1994), and Serpens (Lodieu et al. 2002a). Wilking et al. (2004) have recently set an upper limit of $\alpha \leq 1.6$

on the mass spectrum for NGC1333 across the hydrogen burning limit based on a spectroscopic sample of 25 brown dwarf candidates.

- The Trapezium Cluster lies within the central region of the Orion Nebula Cluster and is the most extensively studied young cluster. The cluster is young (~ 1 Myr), nearby (450 pc), rich and dense ($\sim 10^4$ pc $^{-3}$) and harbours a wide range of stellar masses from $50 M_{\odot}$ to few Jupiter masses. Furthermore, its location in front of molecular cloud minimises the background contamination, making objects with a small extinction likely members.

Multiple surveys at various wavelengths have been conducted in the region, including proper motion (Jones & Walker 1988), optical images from the ground (Herbig & Terndrup 1986) and from space (Luhman et al. 2000), infrared surveys (McCaughrean & Stauffer 1994) complemented by spectroscopy (Hillenbrand 1997; Lucas et al. 2001) to infer masses and ages for each individual member.

Hillenbrand (1997) inferred a IMF which peaks at about $0.2 M_{\odot}$ and declines towards lower masses. The extension of this work to the substellar regime confirmed the previous conclusions (Luhman et al. 2000; Slesnick et al. 2004). Muench et al. (2002) reported a similar IMF from B stars down to the deuterium-burning limit by modelling the infrared luminosity function (Table 1.1 and filled circles with solid line in Figure 1.7).

- The σ Orionis cluster, located around the O9.5 star of the same name, belongs to the Orion OB 1b association. The X-ray detection of a high concentration of sources around the star σ Ori by ROSAT (Walter et al. 1994) triggered deep optical surveys dedicated to the low-mass component of the cluster. The cluster is 1–8 Myr old (Béjar et al. 1999), located at 352 pc according to *Hipparcos* (Perryman et al. 1997), and suffers from little reddening (Lee 1968).

A deep optical (R , I , and Z) survey of a ~ 850 arcmin 2 area in the cluster with additional near-infrared photometry revealed numerous low-mass stars, brown dwarfs (Béjar et al. 1999), and planetary-mass objects (Zapatero Osorio et al. 2000). Many objects have been spectroscopically confirmed over a large mass range in the optical (Barrado y Navascués et al. 2001b) and in the near-infrared (Martín et al. 2001). The cluster mass function, derived from low-mass stars ($0.2 M_{\odot}$) down to the deuterium-burning limit, indicates a rising slope with an index $\alpha = 0.8 \pm 0.4$ (Béjar et al. 2001), when expressed as the mass spectrum (Table 1.1 and open triangle with solid line in Figure 1.7).

- IC 348 is located on the northeast end of the Perseus molecular cloud complex. The cluster is young (1–3 Myr), relatively nearby ($d \sim 315$ pc), rich (about 400 members), compact ($D \sim 20'$) with low extinction ($< A_V > = 0\text{--}5$ mag). IC348 has been extensively targeted in the past to extract cluster members via proper motion (Fredrick 1956), H α emission (Herbig 1998), infrared luminosity functions (Lada & Lada 1995), and optical colour-magnitude diagrams (Herbig 1998; Luhman 1999).

Tej et al. (2002) recently derived a cluster mass function from all-sky catalogues over the whole cluster area and inferred a power law with an index $\alpha = 0.8 \pm 0.2$. Luhman et al. (2003b) assigned spectral types, effective temperatures, and masses for a large number of members within the central $42' \times 28'$ area in the cluster to construct an extinction-limited sample ($A_V \leq 4$) from B stars to late-M dwarfs. The cluster mass function rises from high-mass stars down to $1 M_{\odot}$, rises more slowly to peak at $0.1\text{--}0.2 M_{\odot}$, and declines towards the substellar regime in logarithmic scale (Table 1.1 and histogram with solid line in Fig-

ure 1.7). The IMF derived from the modelling of the luminosity function of a 20.5 arcmin² region confirmed those results (Muench et al. 2003).

- Taurus is a young (1–2 Myr), nearby ($d \sim 140$ pc), low-density ($n \sim 1\text{--}10 \text{ pc}^{-3}$) star-forming region located above the galactic plane ($b \sim 20^\circ$). The total extent of the Taurus region on the sky is about 100 deg². However, 60 % of the pre-main-sequence stars are concentrated in six groups with an average radius of about one parsec (25' on the sky).

Combining previous studies (Briceño et al. 1998; Luhman 2000) with a new optical and near-infrared wide-field survey of 8.4 square degrees in Taurus, Briceño et al. (2002) selected an extinction-limited ($A_V \leq 4$) sample of spectroscopically confirmed members down to $20 M_{\text{Jup}}$. Luminosities, effective temperatures, and masses were inferred for each individual member based on their location in the H-R diagram. Briceño et al. (2002) and Luhman et al. (2003a) concluded that the Taurus IMF peaks at about $0.8 M_{\odot}$ and declines more sharply than the Trapezium Cluster towards low-mass and high-mass stars, yielding a deficit of brown dwarfs and stars more massive than $1 M_{\odot}$ in logarithmic scale (Table 1.1 and histogram with dashed line in Figure 1.7).

- The ρ Ophiuchus dark cloud contains a young (< 1 Myr), nearby ($d = 160$ pc), and compact ($D = 20'$) population of low-mass stars. The region has been extensively targeted in the near-infrared (e.g. Rieke & Rieke 1990), in the mid-infrared (e.g. Bontemps et al. 2001), and in the X-rays (Vuong et al. 2003) due to large extinction (A_V up to 50 mag) hampering optical observations. Near-infrared spectroscopy is available for a large number of low-mass stars, including possible brown dwarfs (e.g. Greene & Lada 1996).

Luhman & Rieke (1999) inferred a complete IMF down to $\sim 0.08 M_{\odot}$ from a compilation of new spectroscopic data and previous surveys. They concluded that the IMF for the studied region in ρ Oph matches that of Miller & Scalo (1979) at masses above $0.4 M_{\odot}$ and slowly declines to the hydrogen-burning limit, in agreement with a flat IMF found by Comerón et al. (1993). These results are consistent with logarithmic IMF determinations in the Trapezium Cluster and IC348 using similar methods to infer luminosities and masses for cluster members (Luhman et al. 2000).

- Chameleon is a young (1–2 Myr) and nearby ($d \sim 160$ pc) star-forming region with an angular size of about 3 square degrees (Boulanger et al. 1998) composed of several clouds (Wichmann et al. 1998). The relatively high galactic latitude and moderate extinction makes the region amenable to unveil brown dwarfs with X-ray (Neuhäuser & Comerón 1998), near-infrared (Cambresy et al. 1998), and mid-infrared (Persi et al. 2000) observations.

A deep H α survey combined with near-infrared imaging of a 300 arcmin² area in the most obscured region of the Chameleon cloud revealed 22 members less massive than $1 M_{\odot}$ (Comerón et al. 1999; Comerón et al. 2000). The derived mass function, although affected by small statistics, is in agreement with estimates in other star-forming regions (Comerón et al. 2000). A wide-field near-infrared survey of about one square degree in Chameleon has extracted an additional set of about 100 members spanning $K = 12\text{--}16$ mag, on the basis of their colour excess (Gómez & Kenyon 2001). Similarly, photometry from the DENIS survey has extracted new members, including possible brown dwarfs (Vuong et al. 2001).

1.5.4 Brown dwarfs in young open clusters

In the previous section, we have focussed on star-forming regions and embedded clusters to indicate the advantages compared to the solar neighbourhood. We will emphasise here the significant advantages (+) and drawbacks (−) of young open clusters (50–200 Myr) compared to the field and star-forming regions:

- + Open clusters are equidistant, coeval sample of stars with a similar chemical composition within a limited area on the sky as star-forming regions.
- + Brown dwarfs are brighter at young ages. They are obviously brighter in star-forming regions than in open clusters but the distance comes into play as well.
- + Mass segregation and evaporation of the less massive components affects clusters older than ~ 200 Myr, not of interest within the framework of this thesis.
- Larger distances than nearby stars implies a lower sensitivity to low-mass stars. This effect is often compensated by the youth of open clusters.
- Contamination by field stars is the biggest disadvantage of open clusters particularly at the faint end, yielding large incompleteness in the substellar regime.
- Incompleteness in the high-mass regime because of the short lifetime of high-mass stars. This point and the previous one constitute arguments in favour of the studies directed towards star-forming regions and massive clusters.

Most of the surveys have concentrated on nearby and young open clusters to investigate the substellar mass function. Only four open clusters younger than 200 Myr are closer than 200 pc: the Pleiades, α Per, IC2602, and IC2391. We will emphasise below the Pleiades and α Per clusters for which substellar mass function estimates are available (Figure 1.8).

The Pleiades open cluster is by far the best studied open cluster and the ideal place to reveal very low-mass stars and brown dwarfs. As a consequence, Rebolo et al. (1995) unearthed the first cluster brown dwarf, Teide 1, followed by many others over the last few years (e.g. Bouvier et al. 1998 and references therein). The reasons for the large number of surveys targeting the Pleiades are the following:

1. The Pleiades is a rich cluster with approximately 1200 known members.
2. The cluster is relatively nearby with a distance estimated to ~ 130 pc. The isochrone fitting estimate ($d = 128$ pc; Pinsonneault et al. 1998) has been recently confirmed by the orbital solution of a double-lined eclipsing binary ($d = 132$ pc; Munari et al. 2004) compared to the *Hipparcos* distance ($d = 119$ pc; van Leeuwen 1999).
3. The cluster proper motion is $\mu_\alpha = +19$ mas/yr and $\mu_\delta = -43$ mas/yr (Jones 1973) with a radial velocity of 5.9 kms^{-1} (Rosvick, Mermilliod, & Mayor 1992). The motion of the cluster is large enough to disentangle members from field stars.
4. The cluster is relatively compact with the majority of members located within 2.5° of the cluster centre (Pinfield et al. 1998).

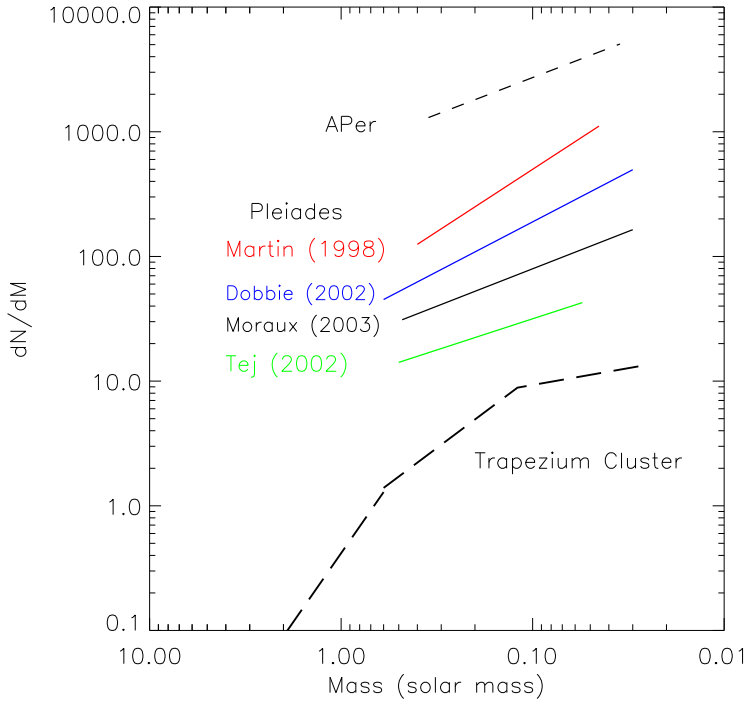


Figure 1.8: Comparison of substellar mass functions, plotted as the mass spectrum, for the Pleiades (Bouvier et al. 1998; Martín et al. 1998; Tej et al. 2002; Dobbie et al. 2002; Moraux et al. 2003), and α Per (Barrado y Navascués et al. 2002) clusters. The mass function estimated by Muench et al. (2002) for the Trapezium Cluster is included for comparison purposes. The different estimates are offset along the y-axis for clarity.

5. The cluster is relatively young. The upper main-sequence turn-off fitting yielded an age of 70 Myr while the lithium test derived an age of 125 Myr (Stauffer et al. 1998).
6. Extinction and reddening towards the cluster are generally uniform ($A_V = 0.12$) and the relatively high galactic latitude ($b = -24^\circ$) reduces the contamination by background objects.

Proper motion studies using multi-epoch photographic plates revealed cluster members down to the hydrogen-burning limit with no significant contamination by background objects (Hambly et al. 1993; Meusinger et al. 1996; Hambly et al. 1999). The search for brown dwarfs in the Pleiades was mainly based on deep optical surveys over small areas on the sky (Bouvier et al. 1998; Zapatero Osorio et al. 1997b; Pinfield et al. 2000) with subsequent near-infrared imaging to weed out contaminating objects (Zapatero Osorio et al. 1997a; Dobbie et al. 2002).

Additional spectroscopic criteria, including $H\alpha$ in emission, lithium in absorption, gravity, radial and rotational velocities have strengthened the membership (Basri et al. 1996; Martín et al. 1996). The large proper motion of the cluster relative to field stars allowed Moraux et al. (2001) to confirm brown dwarf candidates as members over a time baseline of five years.

The numerous surveys quoted below converged towards comparable estimates of the Pleiades mass spectrum (Figure 1.8 and Table 1.1) across the stellar/substellar boundary.

- Martín et al. (1998) derived $\alpha = 1.0 \pm 0.5$ in the $0.40\text{--}0.045 M_{\odot}$ mass range based on a deep survey initiated by Zapatero Osorio et al. (1997b).
- Tej et al. (2002) estimated $\alpha = 0.5 \pm 0.2$ between 0.50 and $0.055 M_{\odot}$ based on a pure statistical approach involving 2MASS and GSC databases.
- Dobbie et al. (2002) inferred $\alpha = 0.8 \pm 0.2$ based on a deep optical photometric survey down to $0.040 M_{\odot}$.
- Moraux et al. (2003) found $\alpha = 0.6 \pm 0.11$ over the $0.48\text{--}0.03 M_{\odot}$ mass range from a complementary deep (I, Z) imaging program to the (R, I) survey by Bouvier et al. (1998).

The α Per cluster is the second best studied open cluster after the Pleiades. Although α Per might be as rich as the Pleiades, the membership list is less complete than the Pleiades for the following reasons:

1. α Per has a small proper motion not well separated from field stars. Hence, proper motion surveys were less frequent and more subject to contamination than in the Pleiades.
2. The cluster is located at low galactic latitude ($b = -7^{\circ}$ versus $b = -24^{\circ}$ for the Pleiades), increasing the contamination by reddened background giants and field stars.
3. α Per is further away than the Pleiades (180 pc versus 130 pc). However, the cluster is younger than its Pleiades counterpart (90 Myr versus 125 Myr), yielding a comparable location of the lithium depletion boundary $I \sim 18.0$.

The reddening to the cluster is low ($A_V = 0.30$) although some spatial variations are seen across the cluster (Prosser 1994). Proper motion studies based on Schmidt plates have provided a large list of probable cluster members (Heckmann et al. 1956; Stauffer et al. 1985; Stauffer et al. 1989b). Colour selection and spectroscopic follow-up were, however, necessary to ascertain the membership of selected candidates due to the small proper motion and low galactic latitude of the cluster (Prosser, 1992, 1994). Surveys conducted in X-rays confirmed the membership of known cluster members (Randich et al. 1996; Prosser et al. 1996b) and unearthed new candidates later assessed as members via photometry and spectroscopy (Prosser & Randich 1998, Prosser et al. 1998).

Recently, Stauffer et al. (1999) applied the lithium test (Rebolo et al. 1992) and inferred an age of 90 ± 10 Myr for the α Per cluster, value twice as large as the upper main-sequence turn-off age (50 Myr). Combining optical and near-infrared imaging, Barrado y Navascués et al. (2002) extracted a list of new cluster members down to $35 M_{Jup}$. The cluster mass function was well approximated by a power law of index $\alpha = 0.59 \pm 0.05$ over the $0.3\text{--}0.05$ mass range, in agreement with the Pleiades estimates (Figure 1.8 and Table 1.1). Additional information on the cluster is provided in Chapter 3.

Other open clusters have been surveyed in details but no mass function estimate has been made available to date. The mass function for the 150–200 Myr old open cluster M35 was derived down to the hydrogen-burning limit (Barrado y Navascués et al. 2001) due to its larger distance ($d \sim 900$ pc). Among open clusters, pre-main-sequence ones are of prime interests, including NGC2547 (20–40 Myr and ~ 400 pc), IC2391 (30–50 Myr and 150 pc), and IC2602 (~ 30 Myr and 150 pc). The large number of cluster members in IC2391 and IC2602 originate from X-rays

surveys with subsequent photometric and spectroscopic assessments. The age of IC2391 was recently derived from the lithium test, yielding a value of 53 Myr (Barrado y Navascués et al. 2001a), larger than the turn-off main-sequence estimate (30 Myr).

The main conclusions of the studies directed towards young open clusters and star-forming regions suggest that the IMF keeps rising in the substellar regime. However, the recent survey conducted in the Taurus cloud indicate a possible variation of the mass function with the environment.

The work presented in this thesis will focus on the search for low-mass stars and brown dwarfs in the solar neighbourhood and in open clusters. Chapter 2 presents the results of a proper motion survey carried out in the southern sky to unearth the closest and coolest neighbours to the Sun. Chapter 3 and Chapter 4 concentrate on the substellar IMF in two young open clusters. In Chapter 3, we will report a near-infrared wide-field survey of the α Per cluster in addition to the recent mass function determination published by Barrado y Navascués et al. (2002). In Chapter 4, we will describe the results of a deep wide-field optical survey with near-infrared follow-up observations of the pre-main-sequence open cluster Collinder 359.